CDF/DOC/MUON/CDFR/8088
Version 1.05
May 16, 2006

High P_T Intermediate Muon (BMU) Reconstruction and Identification with 5.3.3/6.1.2 Data *vs* 5.3.3/6.1.3 MC

Salvador Carrillo[1], Shan-Huei Chuang[2], Nikos Giokaris[3], Arkadios Manousakis-Katsikakis[3], Anyes Taffard[4], Monica Tecchio[5], Fabiola Vázquez[1], Costas Vellidis[3]

[1] Universidad Iberoamericana, Mexico
[2] University of Wisconsin at Madison
[3] University of Athens, Greece
[4] University of Illinois at Urbana-Champaign
[5] University of Michigan at Ann Arbor

Abstract

We studied the reconstruction and identification of muons recorded by the CDF II Intermediate Muon Detector (BMU) and optmized the cuts for high p_t analyses using $Z \to \mu\mu$ data and MC in the conventionally called Gen 5 and Gen 6 run ranges. We generally reach shape agreement in data *vs* MC and understand the few cases of disagreement. We recognize the need of and hence recommend data/MC scale factors to compensate the slight difference of selection efficiencies between data and MC.

Contents

1 Introduction

The detector design of IMU is documented in the CDF II Detector Technical Design Report [1]. The essential barrel of muon chamber (BMU) consists of 2 sides $\times$ 4 layers $\times$ 216 drift tubes with CMP/CMX-like tube design but different tube dimensions and form a top-270° arc in the rapidity range of $1.0 < |\eta| < 1.5$.

IMU is behind toriod steels of 6.2-20 pion interation lengths and the IMU triggers at Level 2 use the timing info from plug/wall hadron calorimeter (PHA/WHA TDC) in addition to barrel/toroid scintillator counters (BSU/TSU), so hadronic punch-through is largely suppressed and BMU fake rate is expected to be low.

Online speaking, IMU = BMU + BSU + TSU; offline, IMU = BMU.

2 Basic Strategy

We exclusively use $Z^0 \rightarrow \mu^+\mu^-$ events with both muon high p_t since this channel is known to contain little background. To minimize the number of unknowns we require one of the $Z \rightarrow \mu\mu$ daughters to be a central muon, either CMUP or CMX as recommended by Joint Physics [3] and described in [4, 5, 7, 8, 10], since the central muon behaviors from trigger level, reconstruction to identification have been substantially understood. The other one has to be a BMU candidate according to the goal of our studies. With one central muon and at least one forward track identified we impose $Z \rightarrow \mu\mu$ event selection cuts and gradually add good BMU selection cuts as studies go on.

2.1 Central Muon Selection

We select the CMUP/CMX central muon with the following cuts:

track $p_t > 20$ GeV/c;

$E_{em} < 2 + \max(0,\ 0.0115\ (p - 100))$ GeV;

$E_{had} < 6 + \max(0,\ 0.028\ (p - 100))$ GeV;

calorimetric isolation fraction < 0.1;

number of COT axial superlayers with at least 5 hits > 2;

number of COT stereo superlayers with at least 5 hits > 1;

track $|z_0| < 60$ cm;

track $|d_0| < 0.(0)2$ cm if with (silicon +) COT hits attached;

$|\Delta x_{\text{CMU}}| < 3$ cm for CMUP;

$|\Delta x_{\text{CMP}}| < 5$ cm for CMUP;

$|\Delta x_{\text{CMX}}| < 6$ cm for CMX;

$\rho_{\text{COT exit}} > 140$ cm for CMX;

run > 154448 or not from the bluebeam section;

run > 150144 for CMX;

not from the keystone or miniskirt sections for CMX;

x-fid$_{\text{CMP}} < 0$ and z-fid$_{\text{CMP}} < -3$ cm for CMUP;

x-fid$_{\text{CMX}} < 0$ and z-fid$_{\text{CMX}} < -3$ cm for CMX.

where the calorimetric isolation fraction is defined as total transverse energy within a cone of radius $\Delta R \equiv \sqrt{\Delta\eta^2 + \Delta\phi^2} = 0.4$ around the track but not including the track divided by track p_t.

2.2 $Z \to \mu\mu$ Event Selection

If one central muon and at least one forward track* are found in event, we loop over all the forward tracks and select $Z \to \mu\mu$ with the following cuts:

not tagged a cosmic event;

$81 < M_{\text{central muon, forward track}} < 101$ GeV;

$\Delta z_0 < 4$ cm;

opposite signs of electric charges.

2.3 BMU Selection

We select BMU with the following cuts, where cut 2-3 are counted as reconstruction, cut 4 an option and cut 5-12 as identification:

1. track $p_t > 20$ GeV/c;
2. track fiducial to the BMU chamber with x-fid < 0 and **corrected** z-fid < -3 cm;
3. a BMU stub;
4. option: number of BMU stub hits $N_{\text{stub hits}} > 2$;
5. $|\Delta x_{\text{BMU}}| < 9$ cm;
6. track $|z_0| < 60$ cm;
7. track $|d_0| < 0.(0)2$ cm if with (silicon +) COT hits attached;
8. on COT track quality:

   opt 1: COT axial/stereo track segments with at least 5 hits:

   $N_{\text{Ax trkSegs}} \geq 1$ and $N_{\text{St trkSegs}} \geq 2$ for $|\eta_{\text{det}}| < 1.25^{\dagger}$;

   $N_{\text{Ax trkSegs}} \geq 1$ and $N_{\text{St trkSegs}} \geq 1$ for $|\eta_{\text{det}}| \geq 1.25$;

   opt 2: COT hit fraction > 0.6;
9. $E_{em} < 2 + \max(0, 0.0115 \times (p - 100))$ GeV;
10. $E_{had} < 6 + \max(0, 0.028 \times (p - 100))$ GeV;
11. on calorimetric isolation:

    opt 1: no requirement;

    opt 2: ${E_t}^{\text{iso4}} < 4$ GeV;

    opt 3: $({E_t}^{\text{iso4}} - 0.35 \times (N_{\text{vtx}} - 1))/p_t < 0.1$;

    opt 4: ${E_t}^{\text{iso4}}/p_t < 0.1$.

    where option 4 is the calorimetric isolation fraction typically used for central muon selection.

*At such a preselection level, a forward track is any track that passes $|\eta| > 0.9$ and $p_t > 10$ GeV cuts.

†There is BSU hardware separation pertaining to trigger level: $|\eta_{\text{BSU}\textbf{Front}}| < 1.25$ and $|\eta_{\text{BSU}\textbf{Rear}}| \geq 1.25$.

On the optional cut 4: at the simulation/production level a BMU stub is kept if it consists of 2 BMU hits synchronized with a BSU hit or if it consists of 3 or 4 BMU hits. As shown in Figure 14, 2-hit BMU stubs are under-simulated. This optional cut will be withdrawn after the problem in 2-hit BMU stubs is fixed. For the moment BMU overall scale factors are provided with and without this optional cut in Section 6.

Other BMU selection cuts will be explained in more detail in Section 4 and 5.

3 Data and MC Description

3.1 Data

We use high p_t $Z \to \mu\mu$ events that passed MUON_CMUP18 or MUON_CMX18 triggers and were recorded by the CDF II detector from March 2003 to September 2005. The event run numbers range from 160533 to 203799. As conventionally the collaboration has done, we separate data into two run ranges by the shutdown in September 2004 and call the pre-shutdown run range Generation 5 (Gen 5) and post-shutdown range Generation 6 (Gen 6):

160533 $\leq$ Gen 5 run number $\leq$ 186598 $\Rightarrow$ production 5.3.3 $\Rightarrow$ dataset **bhmu0d**;

190697 $\leq$ Gen 6 run number $\leq$ 203799 $\Rightarrow$ production 6.1.2 $\Rightarrow$ dataset **bhmu0h**.

203800 $\leq$ Gen 6 run number $\leq$ 210011 $\Rightarrow$ production 6.1.2 $\Rightarrow$ dataset **bhmu0i**.

For the transverse momentum of track in data we apply Larry curvature correction [6].

3.2 MC

We use the following $p\bar{p} \to Z^0 \to \mu^+\mu^-$ PYTHIA 6.216 + cdfSim 5.3.2/5.3.3/6.1.3 Monte Carlo samples for simulation:

ztop0i 5.3.2 MC for the Gen 5 run range, 2M events, $\sigma \cdot B(M_{inv} > 30$ GeV) = 234.2 pb;

ztop8i 5.3.3 MC for the Gen 5 run range, 3M events, $\sigma \cdot B(M_{inv} > 30$ GeV) = 234.2 pb;

ztopci 5.3.3 MC for the Gen 6 run range, 2M events, $\sigma \cdot B(M_{inv} > 30$ GeV) = 234.2 pb;

ztopei 5.3.3 MC for the Gen 6 run range, 2M events, $\sigma \cdot B(M_{inv} > 30$ GeV) = 234.2 pb;

zewk6m 6.1.3 MC for the Gen 6 run range, 4M events, $\sigma \cdot B(M_{inv} > 20$ GeV) = 355.3 pb. This sample is tuned for high luminosity.

We use k-factor = 1.4 to correct for the leading order generation. More information about these samples can be obtained from top/ewk MC coordinators or their MC webpages.

3.3 Good Run Lists

We use the version 10.0a good run generating tools provided by the Data Quality Monitering (DQM) group in [2] to generate CMUP-BMU and CMX-BMU good run lists. For each list we require both online and offline CMUP/CMX and IMU bits good according to the RunSummary and obtain the corresponding corrected integrated luminosities as follow:

$$
\begin{aligned}
\text{bhmu0d: } {\mathcal{L}_{int}}^{\text{CMUP-BMU}} &= 246 \pm 14 \text{ pb}^{-1} \\
{\mathcal{L}_{int}}^{\text{CMX-BMU}} &= 231 \pm 13 \text{ pb}^{-1} \\
\text{bhmu0h: } {\mathcal{L}_{int}}^{\text{CMUP-BMU}} &= 440 \pm 26 \text{ pb}^{-1} \\
{\mathcal{L}_{int}}^{\text{CMX-BMU}} &= 410 \pm 24 \text{ pb}^{-1} \\
\text{bhmu0i: } {\mathcal{L}_{int}}^{\text{CMUP-BMU}} &= 240 \pm 14 \text{ pb}^{-1} \\
{\mathcal{L}_{int}}^{\text{CMX-BMU}} &= 235 \pm 14 \text{ pb}^{-1}
\end{aligned}
$$

For reference, the corresponding corrected integrated luminosities for reqruiring only CMUP/CMX bit good are listed below:

$$
\begin{aligned}
\text{bhmu0d: } {\mathcal{L}_{int}}^{\text{CMUP}} &= 378 \pm 22 \text{ pb}^{-1} \\
{\mathcal{L}_{int}}^{\text{CMX}} &= 357 \pm 21 \text{ pb}^{-1} \\
\text{bhmu0h: } {\mathcal{L}_{int}}^{\text{CMUP}} &= 445 \pm 26 \text{ pb}^{-1} \\
{\mathcal{L}_{int}}^{\text{CMX}} &= 416 \pm 25 \text{ pb}^{-1} \\
\text{bhmu0i: } {\mathcal{L}_{int}}^{\text{CMUP}} &= 244 \pm 14 \text{ pb}^{-1} \\
{\mathcal{L}_{int}}^{\text{CMX}} &= 239 \pm 14 \text{ pb}^{-1}
\end{aligned}
$$

3.4 Run Binning

Efficiencies and scale factors are or will be studied on run-dependence with runs binned as in http://www-cdf.fnal.gov/internal/physics/joint_physics/eventyields/runslist.html

	Gen 5 run range	Gen 6 run range
$\epsilon_{\text{CMUP18 trigger}}$	0.9078 ± 0.0047	0.9251 ± 0.0040
$\epsilon_{\text{CMX18 trigger}}$	0.9649 ± 0.0040	0.9586 ± 0.0039
$f_{\text{CMUP REC}\times\text{ID scale}}$	0.8951 ± 0.0059	0.8814 ± 0.0055
$f_{\text{CMX REC}\times\text{ID scale}}$	0.9999 ± 0.0060	0.9795 ± 0.0058

Table 1: CMUP/CMX18 trigger efficiencies and the CMUP/CMX reconstruction and identification overall scale factors for the Gen 5 and Gen 6 run ranges separately [8, 10].

3.5 Weighing Scheme

Each data event is weighed exactly 1. Each MC event is weighed $\epsilon_{\text{CMUP/CMX18 trigger}} \times f_{\text{CMUP/CMX REC}\times\text{ID scale}} \times f_{\text{BMU REC}\times\text{ID scale}} \times \mathcal{L}_{int}{}^{\text{CMUP/CMX-BMU}} \times k\sigma \,/\, N_{\text{events of sample}}$ where the CMUP/CMX18 trigger efficiencies and the (loose, $|\Delta x_{\text{CMU}}| < 3$ cm) CMUP/CMX reconstruction and identification (REC×ID) overall scale factors are summarized in Table 1; other parameters have been stated in previous subsections. The only unknown $f_{\text{BMU REC}\times\text{ID scale}}$ is to be obtained.

4 Reconstruction Efficiencies

The reconstruction efficiency is defined as the probability to find a muon stub and link it to a track. First, to know whether we should find a stub or not in the BMU, we have to know that the muon is fiducial in any of the BMU muon chambers. We use the **MuonFiducialTool** class for this purpose. We define a track as being fiducial in a given muon system if it passes the cuts defined in the next table, and if it passes the requirement of fiduciality as defined by the **MuonFiducialTool** (we will enter in detail of this ahead).

Requierements

First Leg: Muon
The cuts previously defined for the Central Muon Selection.

Second Leg: Track
$p_T > 20.0\ GeV/c$
$E_{EM} < 2 + max(0, (p - 100) \cdot 0.0115) GeV$
$E_{HAD} < 6 + max(0, (p - 1f00) \cdot 0.0028) GeV$
$\|z_0\| < 60.0$ cm
Tracks with no silicon hits: $\|d_0\| < 0.2$ cm
Tracks with silicon hits: $\|d_0\| < 0.02$ cm
different track from first leg
—– COT cut: Option 1 —–
For $\|\eta\| < 1.25$:
Number of axial SL with 5 or more hits ≥ 1 and
Number of stereo SL with 5 or more hits ≥ 2
For $\|\eta\| \geq 1.25$:
Number of axial SL with 5 or more hits ≥ 1 and
Number of stereo SL with 5 or more hits ≥ 1
—– COT cut: Option 2 —–
COT hit fraction > 0.6

Additional cuts
The previously defined $Z \to \mu\mu$ event selection cuts.

We define the reconstruction efficiency as the fraction of stub reconstructed muons in the BMU divided by the tracks that are fiducial in the BMU system.

To be careful not to make any cut selection that will bias the fraction of tracks that reconstruct as a muon, we looked at the efficiency distribution vs the z Fiducial distance in the BMU system. It is important to explain here that for the **MuonFiducialTool** there are two important quantities to consider in order to have fiducial tracks and these are

"XDistance" (this is what we call x Fiducial distance) and "ZDistance" (we refer to this quantity as the z Fiducial distance). The first refers to the distance in the local-x-direction of the chamber (along the drift direction), and the second refers to the local-z-direction of the chamber (parallel to the drift wires, or longitudinal direction). When the track is projected to the plane of the BMU chamber, the fiducial distance is then defined as the distance between the projected track position and the edge of the chamber. For example: z fiducial distance = 0 means the edge of the detector in the z-local distance. A negative value for these distances indicates that the track is inside the chamber (fiducial), while a positive value indicates that the track is outside the chamber (not fiducial). The absolute value of these distances is never larger than 50 cm. A value of +50 in the x Fiducial distance will mean more than 50 cm. OR that the extrapolated track is very far from the detector (it could be very far away in the z-direction, z Fiducial distance is not even calculated in this case). -50 cm. will mean less than -50 cm. A value of +50 in the z Fiducial distance means either the distance was greater than 50 cm. or there were no chambers close enough to measure the distance in the z-direction (x Fiducial distance will be 50 cm. also in the second case). -50 cm. means less than -50 cm. (For a very detailed explanation of these distances and the **MuonFiducialTool** please refer to the file Muon/Muon/MuonFiducialTool.hh)

We will present the distribution of the reconstruction efficiency vs the z fiducial distance for the simulation and the data, we proceed by fixing the x fiducial distance and plot the efficiencies as a function of the z fiducial distance in the following figures:

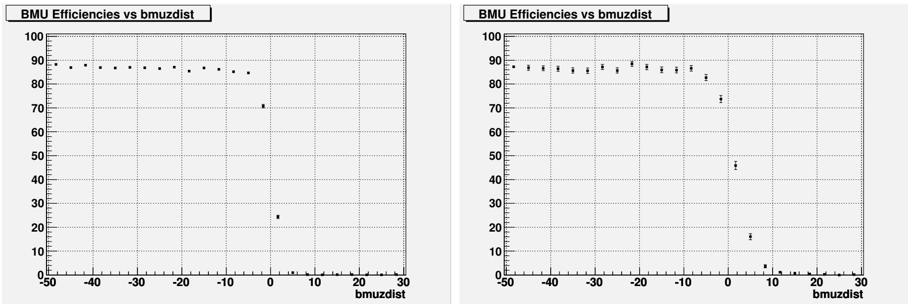

Figure 1: Reconstructed Efficiencies vs z Fiducial distance while x Fiducial < 0, for simulation. Left: Front part of the detector $|\eta| < 1.25$. Right: Rear part of the detector $|\eta| \geq 1.25$

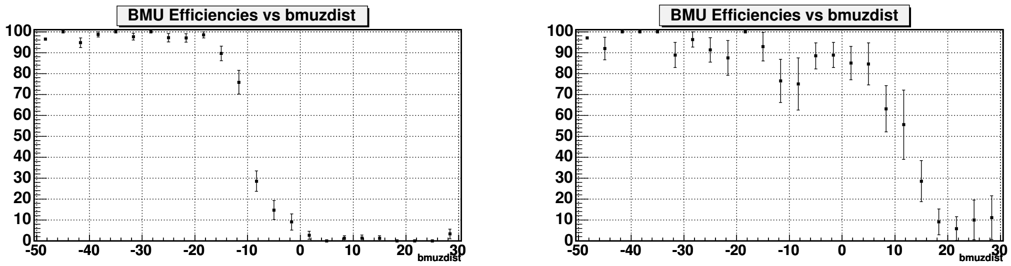

Figure 2: Reconstructed Efficiencies vs z Fiducial distance while x Fiducial < 0, for data (bhmu0d & bhmu0h). Left: Front part of the detector $|\eta| < 1.25$. Right: Rear part of the detector $|\eta| \geq 1.25$

From these plots we can conclude that for the data there exist a geometric shift in the local-z direction of the BMU (the shift is seen in both sides (east and west) of the detector). ‡ There is no evidence of a shift in the simulation.

In the front part of the detector we can see that the efficiency for the z fiducial distance between -10 and 0 (supposedly fiducial) the efficiency is very low, as is for the positive distances in the rest of the plot (not fiducials). On the contrary for the rear part of the detector the efficiency for the z fiducial distance between 0 and +10 is very high, as is for the negative distances in the rest of the plot (fiducials). This result is a strong evidence that exists a shift in the z-direction for the BMU. Our estimate from these plots is 10 cm. We will use this result as a reference for calculating the reconstructed efficiencies.

4.1 Variable Distributions

We will now plot the fiducial distances with respect to the second leg.

The red line shows the fiducial distance for all second legs. The blue area shows after we have applied a requirement that this leg must be linked to a BMU stub. Ideally, one would expect that the blue area would turn off at exactly 0 cm. However, one can see that the turn off is not a strict theta function, instead the distribution fall off over a few centimeters except for the z fiducial distance, in data, which falls off before 0 cm (around -10 cm).

‡See Webtalks WZ Cross Section Working Group 03/14/06 and Lepton Meeting 03/22/06

Also we will plot for the data the same but dividing the sample in terms of the front part of the detector and the rear part, in this way we can conclude also from these plots that there is a shift in the z-direction of the BMU.

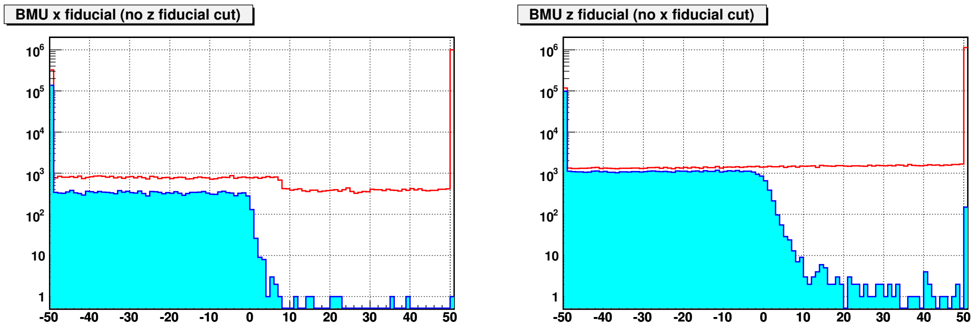

Figure 3: BMU x and z fiducial distances for second leg of $Z \rightarrow \mu^+\mu^-$ events in MC (Gen5). Red: all legs; Blue: BMU muons.

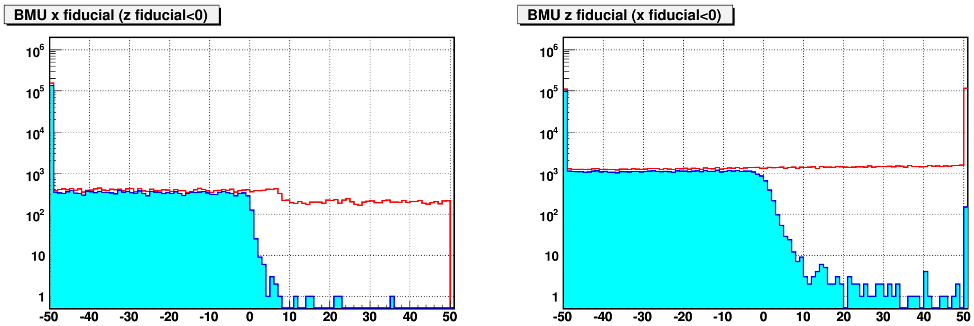

Figure 4: BMU x and z fiducial distances for second leg of $Z \rightarrow \mu^+\mu^-$ events in MC (Gen5). For these plots we have required that the second leg already passes the fiducial cut on the other distance variable, i.e. we have applied a cut of $z < 0$ cm on the x-distance plot and a cut of $x < 0$ cm on the z-distance plot. Red: all legs; Blue: BMU muons.

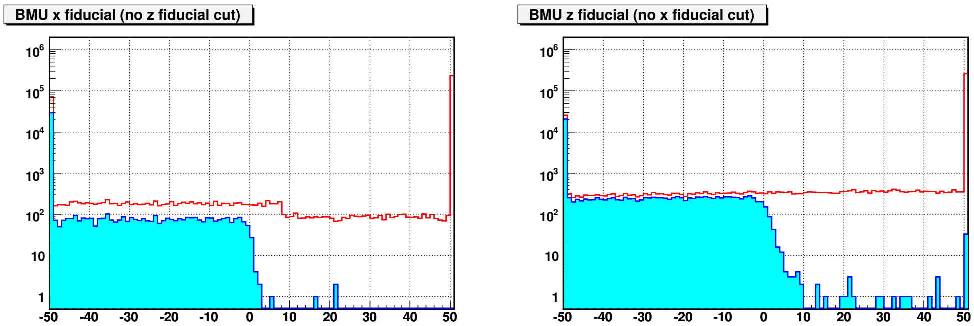

Figure 5: BMU x and z fiducial distances for second leg of $Z \rightarrow \mu^+\mu^-$ events in MC. (zewk6m-Gen6).Red: all legs; Blue: BMU muons.

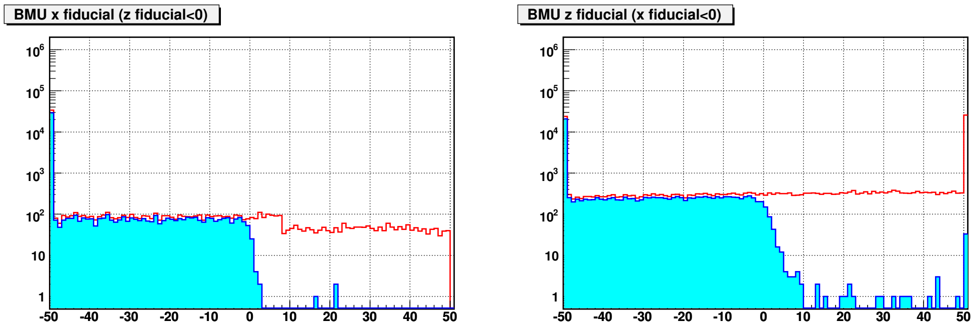

Figure 6: BMU x and z fiducial distances for second leg of $Z \rightarrow \mu^+\mu^-$ events in MC. (zewk6m-Gen6).For these plots we have required that the second leg already passes the fiducial cut on the other distance variable, i.e. we have applied a cut of $z < 0$ cm on the x-distance plot and a cut of $x < 0$ cm on the z-distance plot. Red: all legs; Blue: BMU muons.

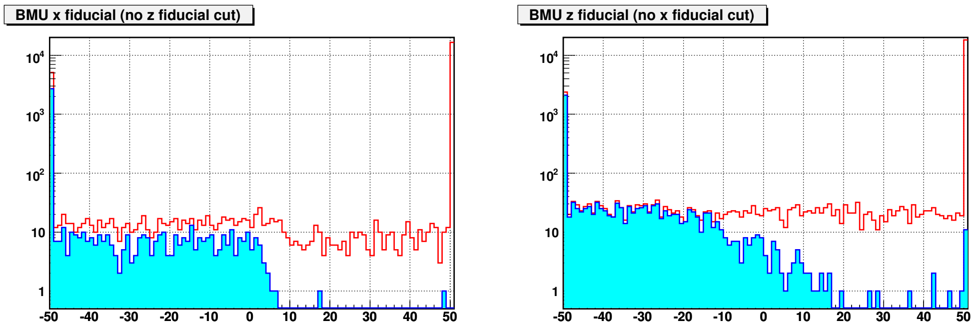

Figure 7: BMU x and z fiducial distances for second leg of $Z \rightarrow \mu^+\mu^-$ events in data. Red: all legs; Blue: BMU muons.

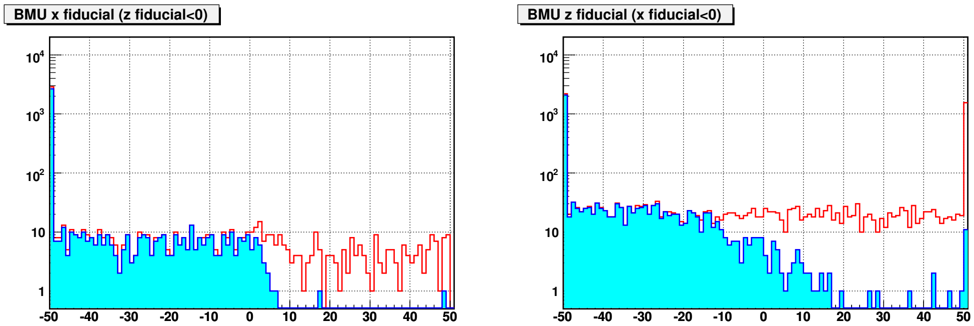

Figure 8: BMU x and z fiducial distances for second leg of $Z \rightarrow \mu^+\mu^-$ events in data. For these plots we have required that the second leg already passes the fiducial cut on the other distance variable, i.e. we have applied a cut of $z < 0$ cm on the x-distance plot and a cut of $x < 0$ cm on the z-distance plot. Red: all legs; Blue: BMU muons.

Our estimate for the edge of the detector in the z-direction is -10 cm. for $|\eta| < 1.25$ and +10 cm. for $|\eta| \geq 1.25$, this translates in terms of the z Fiducial as:

- z Fiducial $<$ -10 cm. for $|\eta| < 1.25$
- z Fiducial $<$ 10 cm. for $|\eta| \geq 1.25$

At this point, we need to take into account also the common requirement for the z fiducial distance, an extra 3 cm inside the edge of the chamber in z direction, as is done for the other muon detectors (CMU, CMP and CMX).

This will change the previous into:

- z Fiducial $<$ -13 cm. for $|\eta| < 1.25$
- z Fiducial $<$ 7 cm. for $|\eta| \geq 1.25$

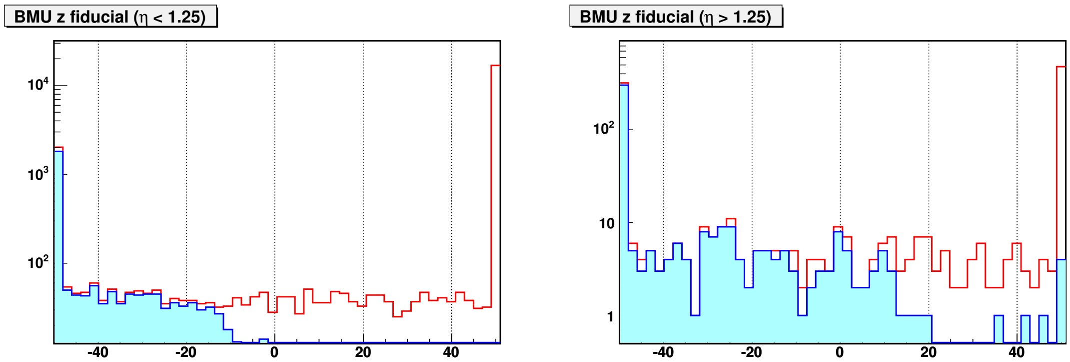

Figure 9: BMU z fiducial distance for the front part and the rear part of the detector, for second leg of $Z \rightarrow \mu^+\mu^-$ events in data. Red: all legs; Blue: BMU muons.

In order to report a Scale Factor to be useful in physics analysis. We decide to propose the following cut for x Fiducial and z Fiducial: (for both: data and MC)

x Fiducial $<$ 0 cm.
z Fiducial $<$ -13 cm. for $\|\eta\| < 1.25$
z Fiducial $<$ -3 cm. for $\|\eta\| \geq 1.25$

With 1st. option COT cut:
(axial and stereo req.)

$\epsilon_{Rec} \pm$ error(%)	muons	tracks	Sample
96.9 $\pm$ 0.5	1037	1070	data:bhmu0d
97.1 $\pm$ 0.4	1847	1902	data:bhmu0h
96.3 $\pm$ 0.6	999	1037	data:bhmu0i
96.9 $\pm$ 0.3	3883	4009	data:full data
87.5 $\pm$ 0.1	43822	50061	MC:ztop8i
87.8 $\pm$ 0.2	23282	26521	MC:ztop0i
87.6 $\pm$ 0.2	35814	40874	MC:ztopci
87.5 $\pm$ 0.2	35609	40716	MC:ztopei
87.6 $\pm$ 0.1	138527	158172	MC:Gen 5
86.4 $\pm$ 0.2	29843	34550	MC:zewk6m
86.4 $\pm$ 0.2	29843	34550	MC:Gen 6

With 2nd. option COT cut:
(expected fraction req.)

ϵ_{Rec} ± error(%)	muons	tracks	Sample
97.3 ± 0.5	1034	1063	data:bhmu0d
97.7 ± 0.3	1844	1888	data:bhmu0h
98.1 ± 0.4	1004	1023	data:bhmu0i
97.7 ± 0.2	3882	3974	data:full data
87.5 ± 0.1	43856	50110	MC:ztop8i
87.8 ± 0.2	23298	26546	MC:ztop0i
87.6 ± 0.2	35866	40935	MC:ztopci
87.5 ± 0.2	35640	40750	MC:ztopei
87.6 ± 0.1	138660	158341	MC:Gen 5
86.4 ± 0.2	29828	34536	MC:zewk6m
86.4 ± 0.2	29828	34536	MC:Gen 6

4.2 Reconstruction Scale Factor

We define the reconstruction scale factor as the ratio between the reconstruction efficiency calculated in the data and the reconstructed efficiency calculated in the MC.

BMU reconstruction efficiencies scale factors		
1st. option COT cut: (axial and stereo req.)		
bhmu0d	bhmu0h	bhmu0i
1.1061 ± 0.0058	1.1238 ± 0.0053	1.1153 ± 0.0072
2nd. option COT cut: (expected fraction req.)		
bhmu0d	bhmu0h	bhmu0i
1.1107 ± 0.0058	1.1308 ± 0.0043	1.1363 ± 0.0055

The reconstruction efficiency is $\sim 10\%$ lower in MC than in data. Our current efforts are towards the understanding of this difference in order that the next simulation release can include a fix.

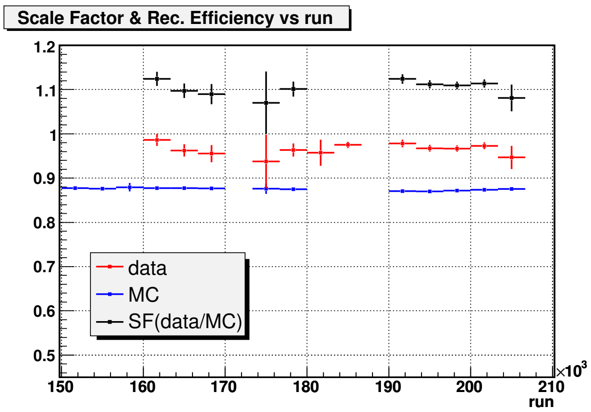

Figure 10: BMU reconstruction efficiency and SF *vs* run range.

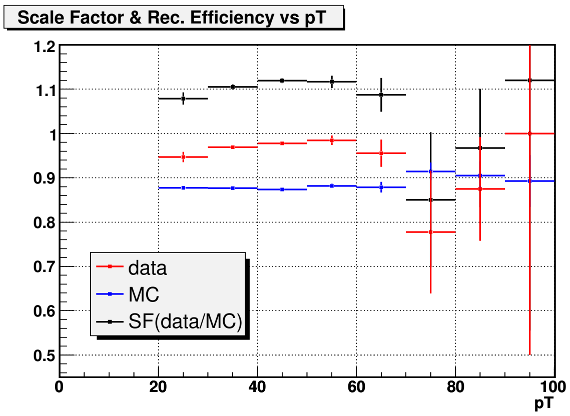

Figure 11: BMU reconstruction efficiency and SF *vs* P_T.

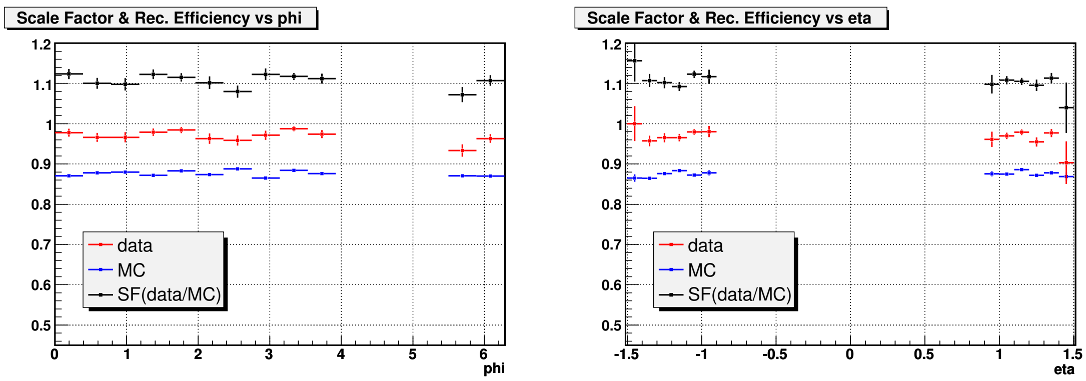

Figure 12: BMU reconstruction efficiency and SF *vs* ϕ & η .

5 Identification

There is small misalignment of x_{BMU} in data, as shown in Figure 15, 16 and 17. Through private communication with J. Bellinger, we have understood that the misalignment is due to some B0 mounting bracket and hence is in all r, ϕ and z directions. Corrections for the mounting bars have been worked out.

On the COT track quality cut options, we extend the concept central muons have used for long in option 1, that is number of good COT track segments $\gtrsim$ 60% the expected value, where good means at least 5 hits. The option 1 cut should be most implementable for analyses since the cut variables most likely have existed for central muon selections. Additionally we adopt a new concept originally proposed by C. Hays in option 2, that is number of COT track hits $\gtrsim$ 60% the expected value[§]. The option 2 cut variable, COT hit fraction, is smooth and even no matter complete or how incomplete COT track coverage, in contrast to the number of good COT track segments.

As shown in Figure 23, COT hit fraction is over-optmistically simulated no matter in the east or west side in 5.3.3 MC; this variable is modelled OK in 6.1.3 MC.

The smallest number of COT track hits is 22 in data and 17 in MC after all the BMU selection cuts.

Among the BMU-pointing tracks, $\sim$ 93% are DefTracks; 6-7% are IO tracks that compensate the lack of DefTracks in the IMU rear regions. 0.05% (negligible and not in use by BMU) are SiSA tracks. See Figure 20.

COT track χ^2 per degree of freedom (χ^2/DoF) $\equiv$ track χ^2 / (number of hits $-$ 5) is plotted in Figure 32, 33 and 34 for reference. If we want to maintain 99% χ^2/DoF cut efficiency for BMU, we should require

χ^2/DoF < 12 for Gen 5 data, $\epsilon = 99.01 \pm 0.26$ %;

χ^2/DoF < 13 for Gen 6 data, $\epsilon = 99.01 \pm 0.20$ %;

option.: χ^2/DoF < 7 for MC, $\epsilon = 99.01 \pm 0.06$ %;

on top of all the BMU reconstruction and identification cuts.

BMU energy deposit through the detector gaps between PHA and WHA is under-simulated in cdfSim, as shown in Figure 25. Although, we place a rather loose upper cut on E_{had} that is far off the under-simulated low E_{had} region.

On the calorimetric isolation cut options, in addition to no isolation cut (opt 1) and fraction ${E_t}^{\text{iso4}}/p_t < 0.1$ (opt 4) that central muons have used for long, we investigate ${E_t}^{\text{iso4}} < 4$ GeV (opt 2) and $({E_t}^{\text{iso4}} - 0.35 \times (N_{\text{vtx}} - 1))/p_t < 0.1$ (opt 3) that is known less dependent on instantaneous luminosity. The difference among these calorimetric isolation cut options can be seen in Figure 37-42 and Table 2-9.

5.1 Variable Distributions

BMU identification cut variables are plotted in Figure 13-32.

[§] One way of getting the expected number of COT track hits is CdfTrack::lastLayerCT() + 1;

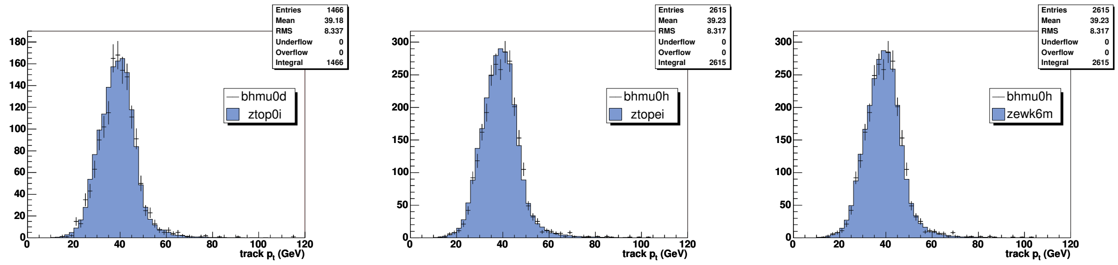

Figure 13: BMU track p_t with 5.3.3/6.1.2 data *vs* 5.3.3/6.1.3 MC.

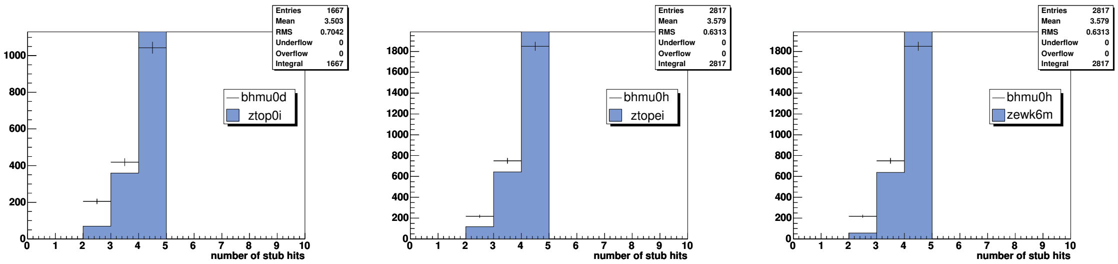

Figure 14: Number of BMU stub hits with 5.3.3/6.1.2 data *vs* 5.3.3/6.1.3 MC.

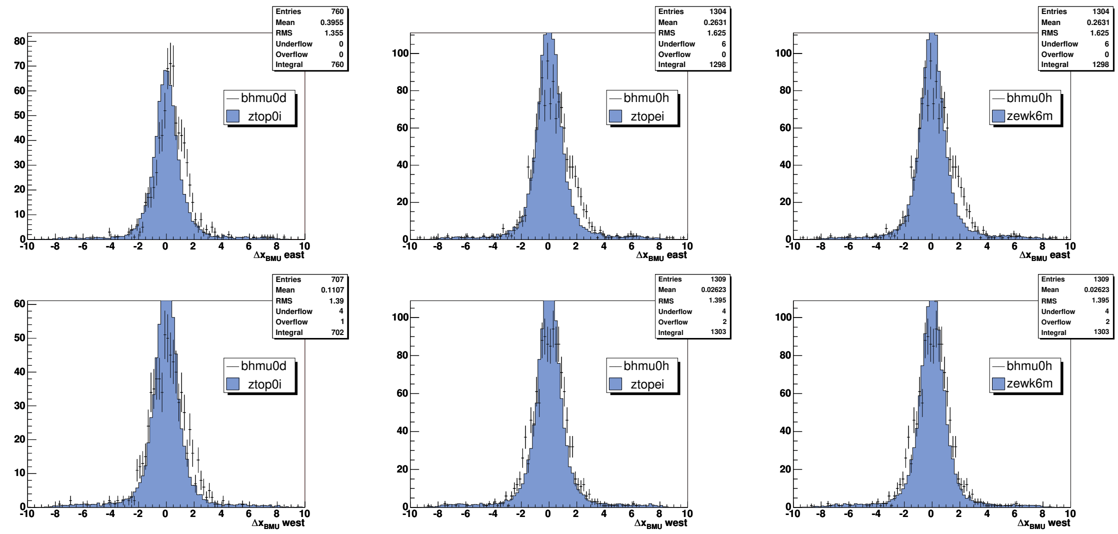

Figure 15: East/west (upper/lower row) Δx_{BMU} with 5.3.3/6.1.2 data *vs* 5.3.3/6.1.3 MC.

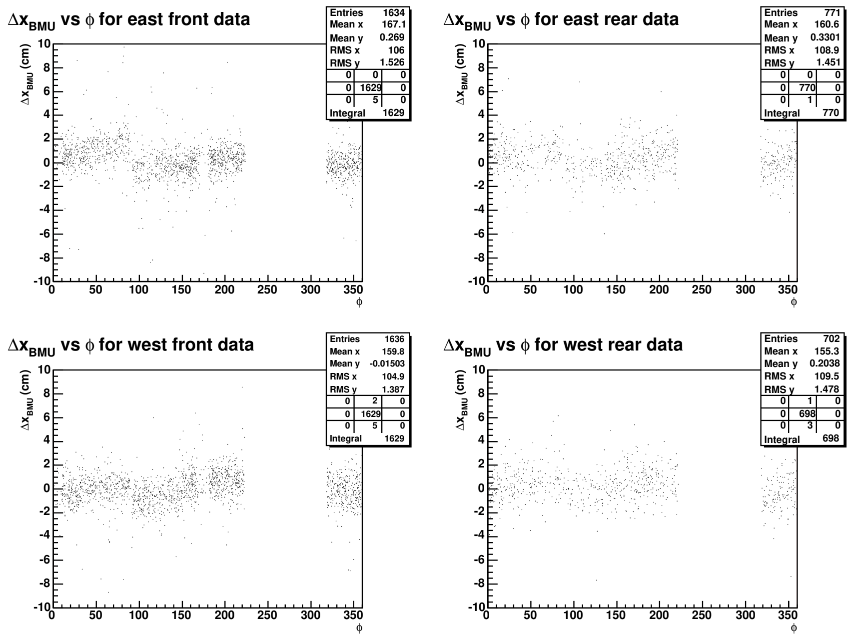

Figure 16: East/west front/rear Δx_{BMU} *vs* ϕ in 5.3.3+6.1.2 data.

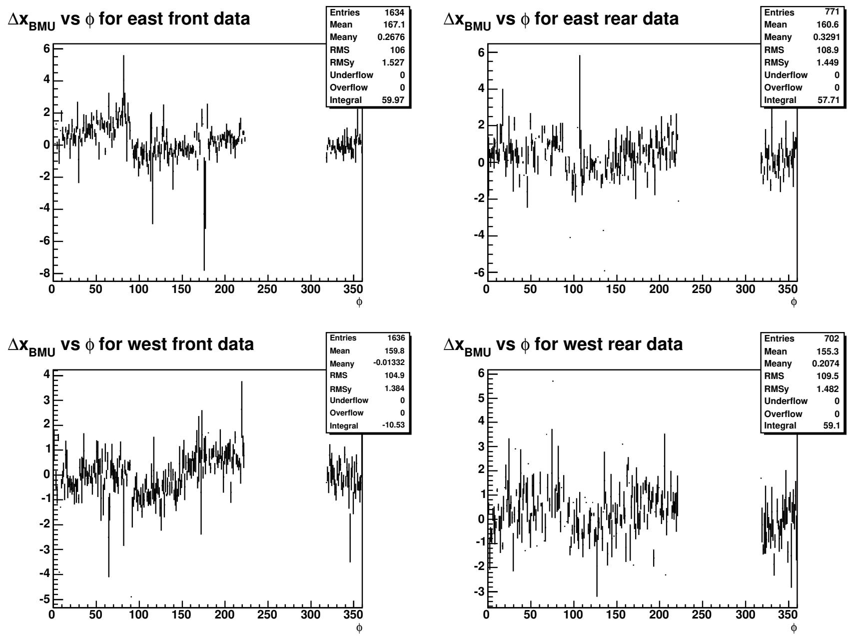

Figure 17: East/west front/rear Δx_{BMU} profile *vs* ϕ in 5.3.3+6.1.2 data.

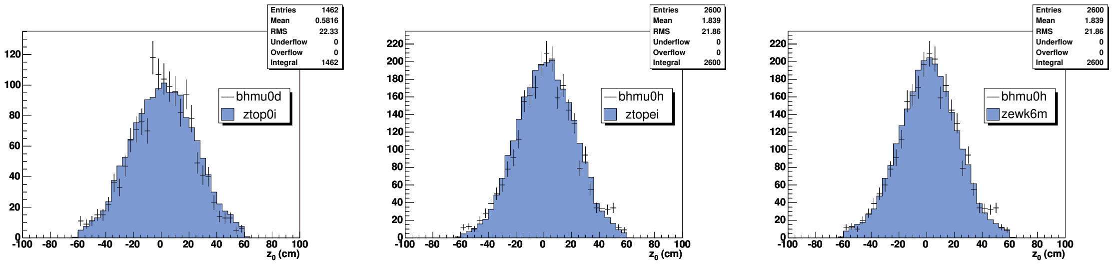

Figure 18: BMU track z_0 with 5.3.3/6.1.2 data *vs* 5.3.3/6.1.3 MC.

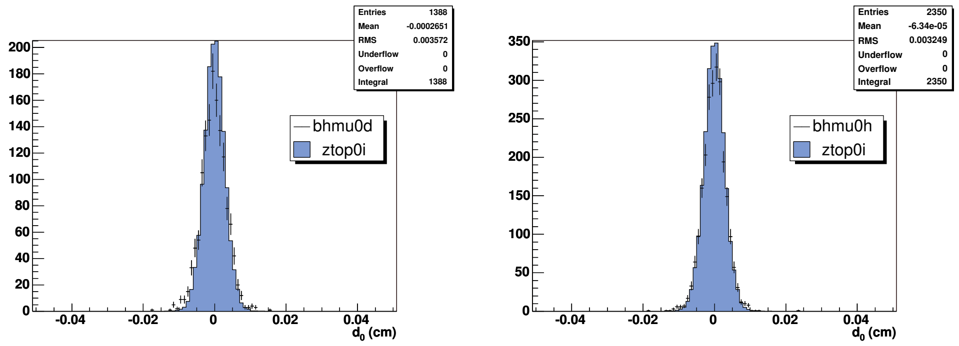

Figure 19: BMU track d_0 with 5.3.3/6.1.2 data *vs* 5.3.3 MC.

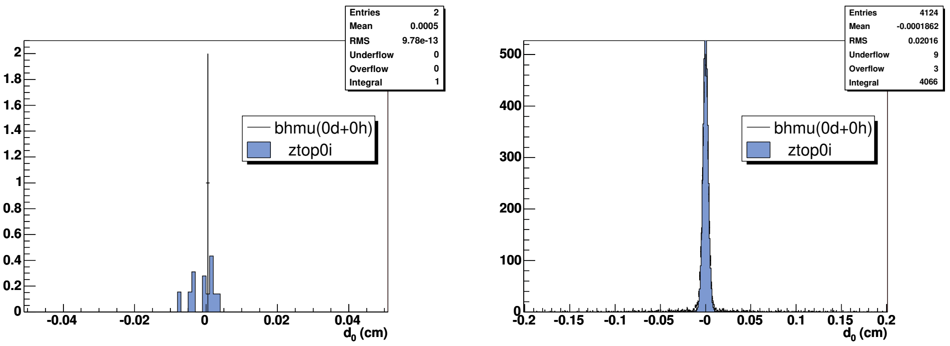

Figure 20: Silicon stand-alone (SiSA, left) or (silicon+)COT (Def+IO, right) candidate BMU track d_0 of after all but the impact parameter and COT track quality cuts with 5.3.3+6.1.2 data *vs* 5.3.3 MC.

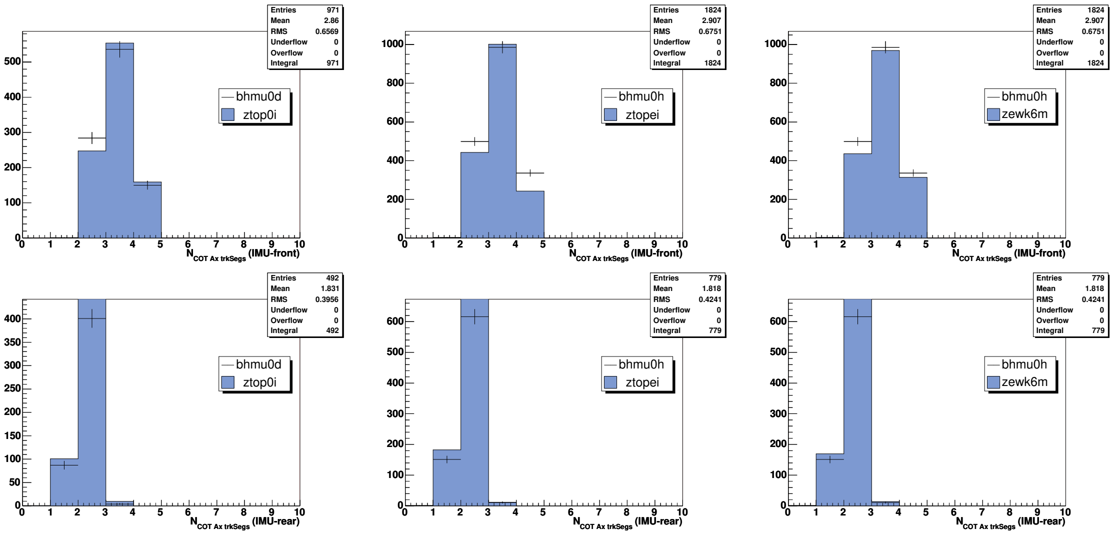

Figure 21: BMU front/rear (upper/lower row) number of good COT axial track segments with 5.3.3/6.1.2 data *vs* 5.3.3/6.1.3 MC.

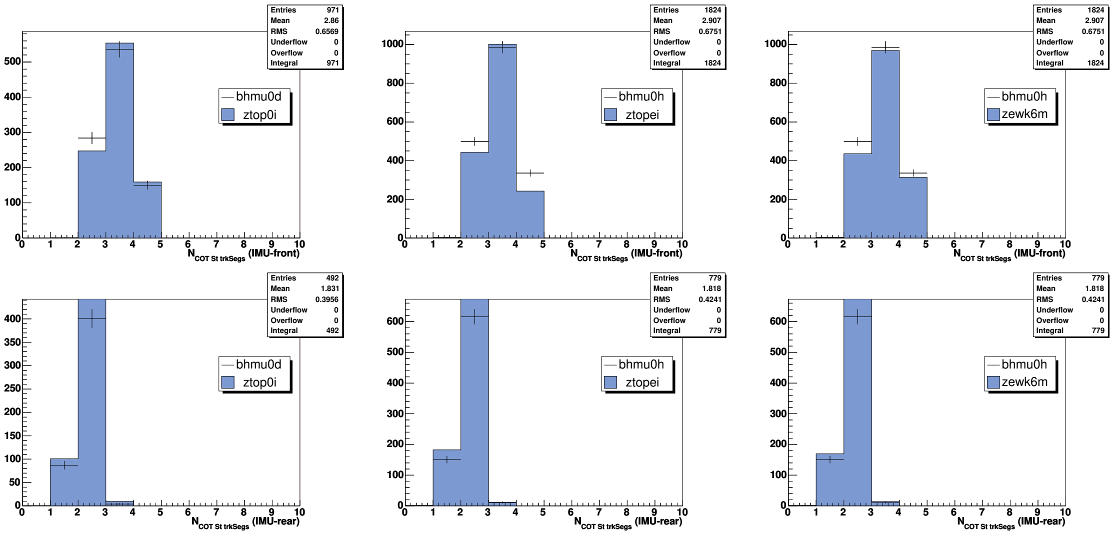

Figure 22: BMU front/rear (upper/lower row) number of good COT stereo track segments with 5.3.3/6.1.2 data *vs* 5.3.3/6.1.3 MC.

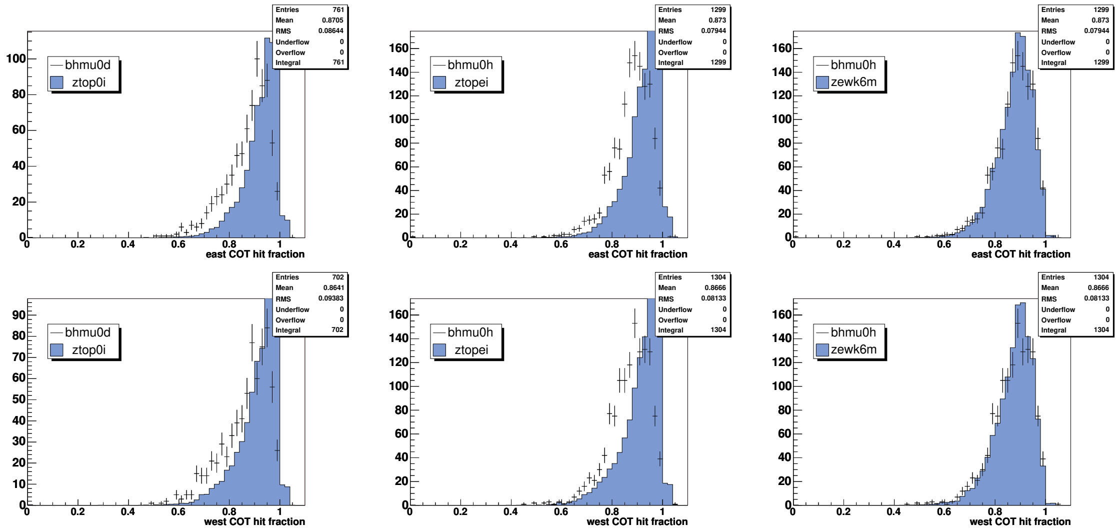

Figure 23: East/west (upper/lower row) COT hit fraction of BMU track with 5.3.3/6.1.2 data *vs* 5.3.3/6.1.3 MC.

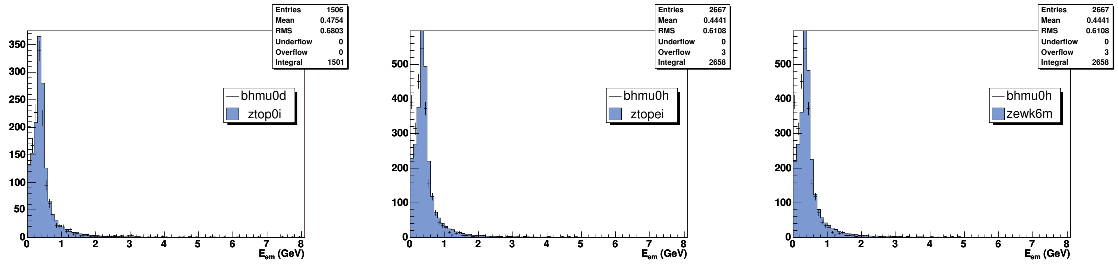

Figure 24: BMU electromagnetic calorimetric energy deposit E_{em} with 5.3.3/6.1.2 data *vs* 5.3.3/6.1.3 MC.

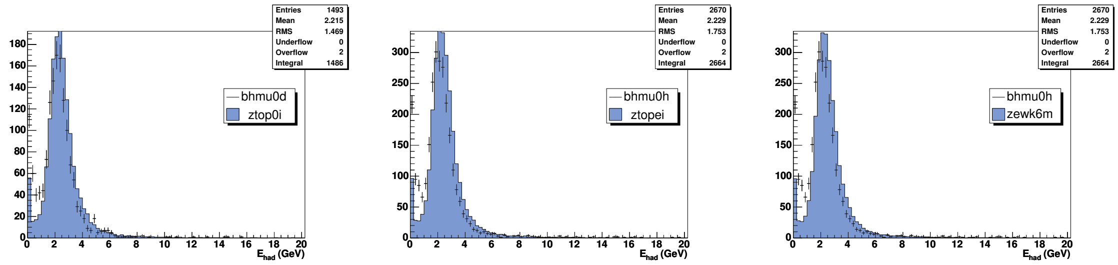

Figure 25: BMU hadronic calorimetric energy deposit E_{had} with 5.3.3/6.1.2 data *vs* 5.3.3/6.1.3 MC.

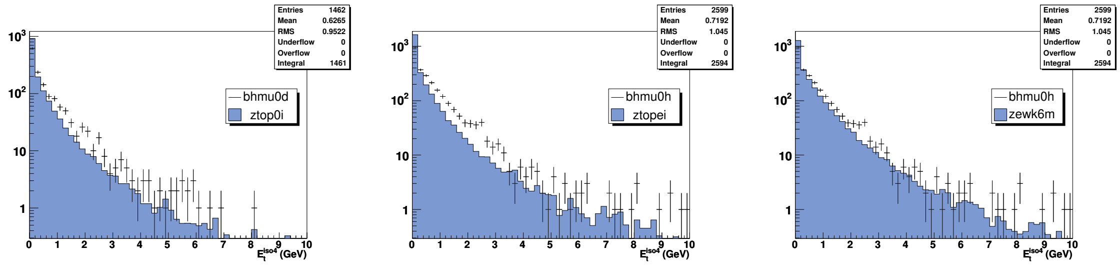

Figure 26: BMU calorimetric isolation energy E_t^{iso4} for 5.3.3/6.1.2 data *vs* 5.3.3/6.1.3 MC.

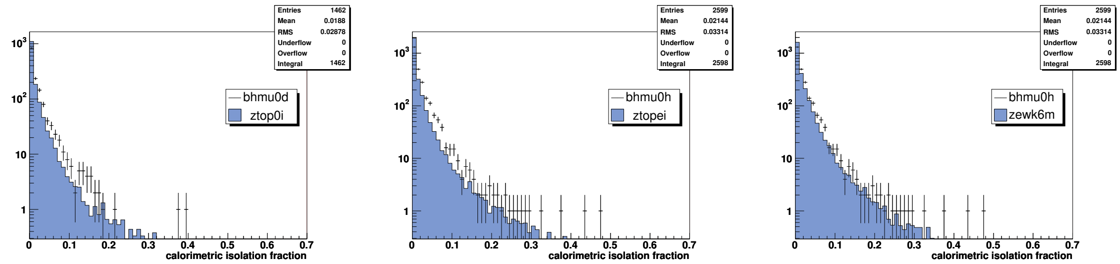

Figure 27: BMU calorimetric isolation fraction with 5.3.3/6.1.2 data *vs* 5.3.3/6.1.3 MC.

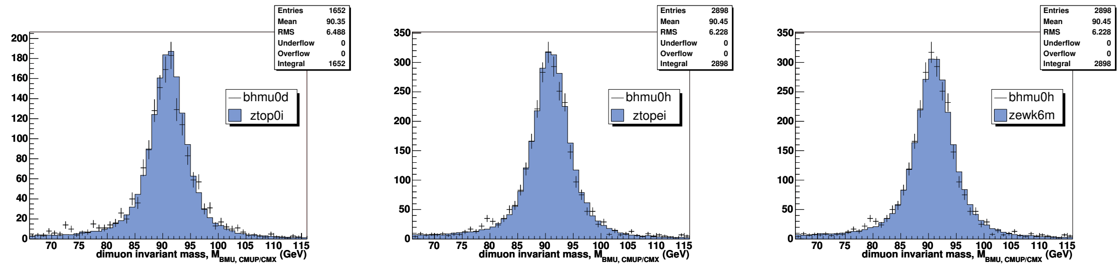

Figure 28: $M_{\text{CMUP/CMX,BMU}}$ after all reconstruction, $N_{\text{stub hits}} > 2$ and identification cuts but not the M_Z window cut with 5.3.3/6.1.2 data *vs* 5.3.3/6.1.3 MC.

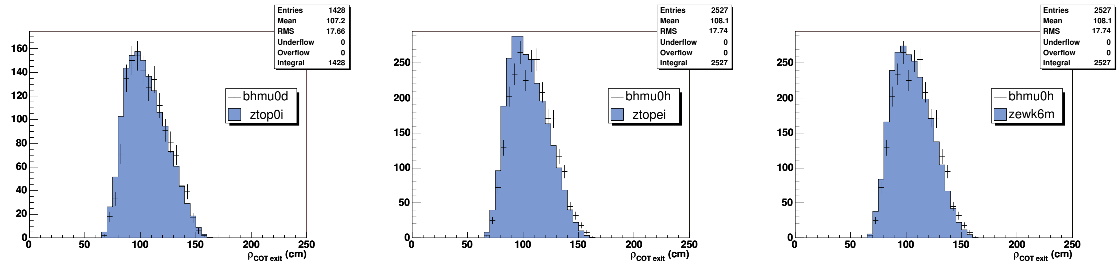

Figure 29: COT exit radius of BMU track with 5.3.3/6.1.2 data *vs* 5.3.3/6.1.3 MC.

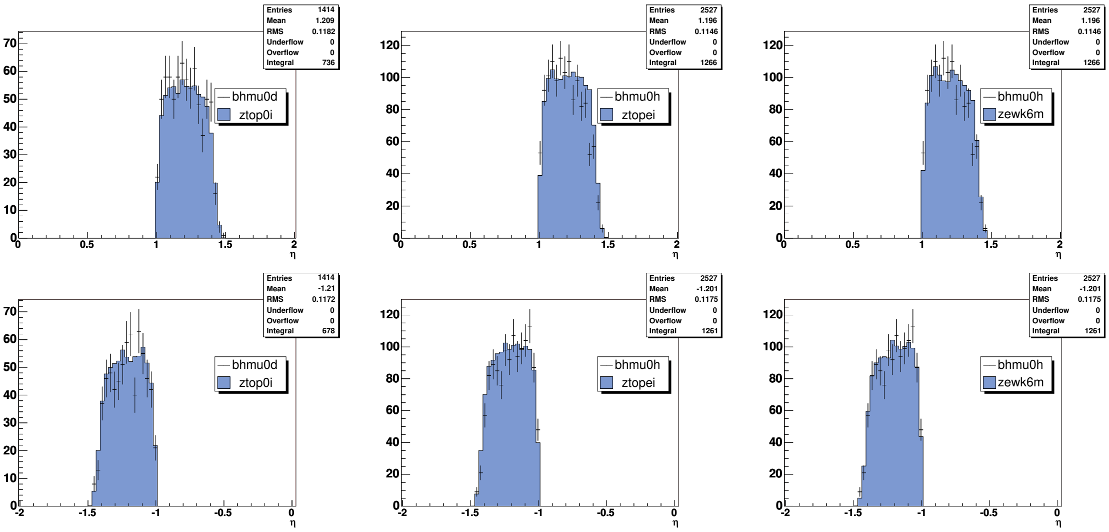

Figure 30: BMU track η with 5.3.3/6.1.2 data *vs* 5.3.3/6.1.3 MC.

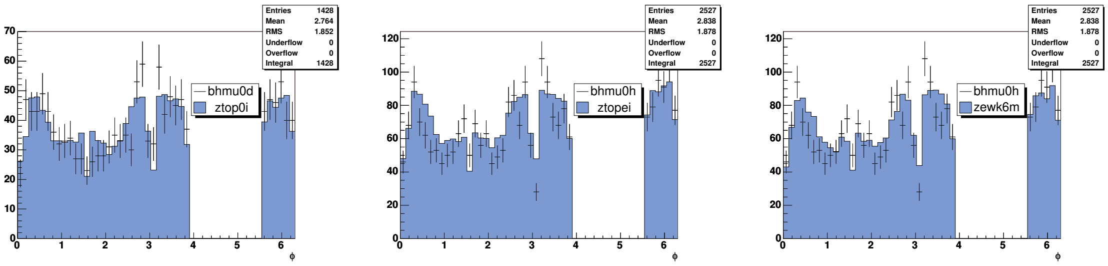

Figure 31: BMU track ϕ with 5.3.3/6.1.2 data *vs* 5.3.3/6.1.3 MC.

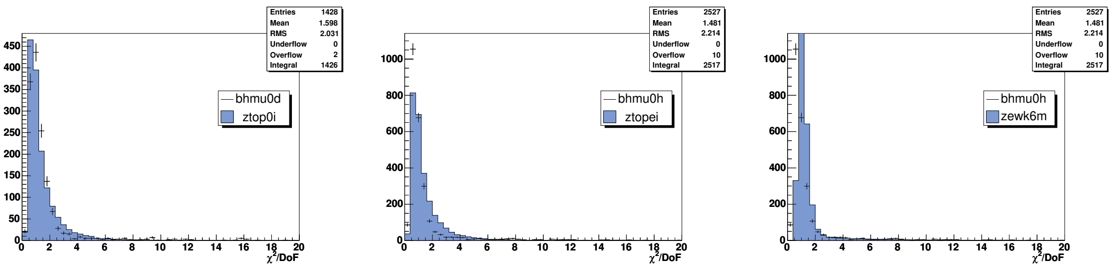

Figure 32: COT χ^2/DoF of BMU track with 5.3.3/6.1.2 data *vs* 5.3.3/6.1.3 MC.

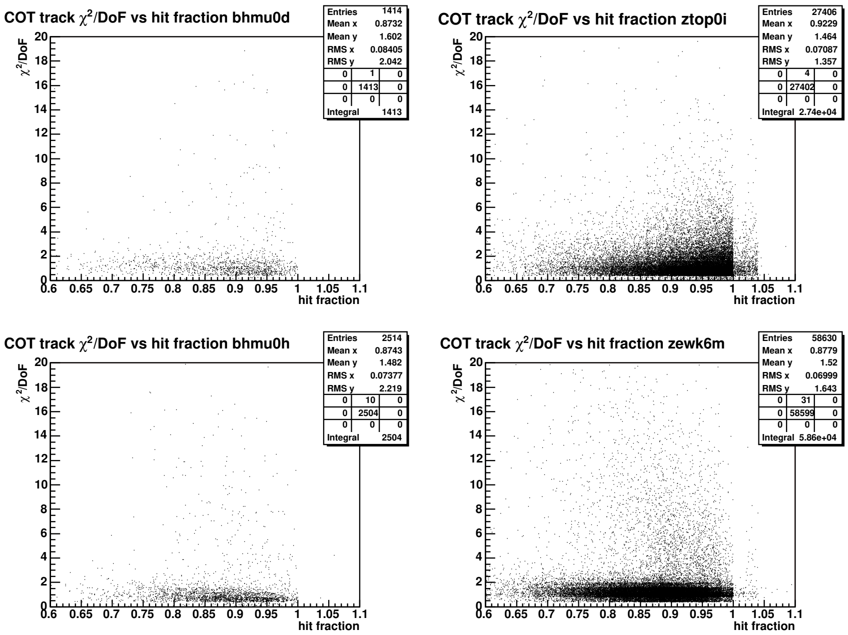

Figure 33: COT χ^2/DoF *vs* hit fraction of BMU track with 5.3.3/6.1.2 data *vs* 5.3.3/6.1.3 MC.

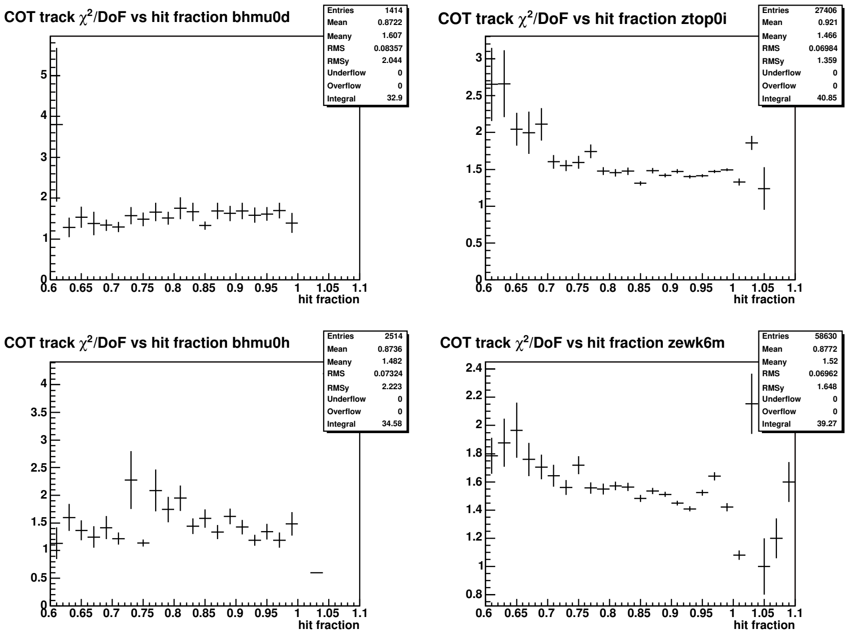

Figure 34: COT χ^2/DoF profile *vs* hit fraction of BMU track with 5.3.3/6.1.2 data *vs* 5.3.3/6.1.3 MC.

5.2 Cut Efficiencies

BMU identification cut efficiencies are listed in Table 2 for the Gen 5 run range and Table 3 and Table 4 for the Gen 6 run range. BMU identification efficiency and scale factor dependencies on track p_t, $\eta_{\rm det}$, ϕ, number of Z vertices, instantaneous luminosity or run range are shown in Figure 35-42.

	data: bhmu0d		MC: ztop0i	
	N_{event}	$\epsilon_{\text{ID}}\pm$ error (%)	N_{event}	$\epsilon_{\text{ID}}\pm$ error (%)
$N_{\text{stub hits}} > 2$		87.72 ± 0.78		95.66 ± 0.12
	1564		29962	
Δx_{BMU}	1558	99.62 ± 0.16	29914	99.84 ± 0.02
d_0	1544	98.72 ± 0.28	29801	99.46 ± 0.04
track quality opt 1	1562	99.87 ± 0.09	29940	99.93 ± 0.02
track quality opt 2	1545	98.79 ± 0.28	29870	99.69 ± 0.03
E_{em}	1517	96.99 ± 0.43	28892	96.43 ± 0.11
E_{had}	1532	97.95 ± 0.36	29179	97.39 ± 0.09
isolation opt 1	1564	100.00 ± 0.000	29962	100.00 ± 0.000
isolation opt 2	1534	98.08 ± 0.35	29588	98.75 ± 0.06
isolation opt 3	1534	98.08 ± 0.35	29469	98.35 ± 0.07
isolation opt 4	1525	97.51 ± 0.39	29468	98.35 ± 0.07
total (trq1×iso1)	1462	93.48 ± 0.62	27894	93.10 ± 0.15
total (trq1×iso2)	1435	91.75 ± 0.70	27573	92.03 ± 0.16
total (trq1×iso3)	1435	91.75 ± 0.70	27471	91.69 ± 0.16
total (trq1×iso4)	1428	91.30 ± 0.71	27470	91.68 ± 0.16
total (trq2×iso1)	1448	92.58 ± 0.66	27829	92.88 ± 0.15
total (trq2×iso2)	1421	90.86 ± 0.73	27510	91.82 ± 0.16
total (trq2×iso3)	1421	90.86 ± 0.73	27407	91.47 ± 0.16
total (trq2×iso4)	1414	90.41 ± 0.74	27406	91.47 ± 0.16

Table 2: BMU identification cut efficiencies for Gen 5 data *vs* 5.3.3 MC, where trq$ stands for the COT track quality option (track quality opt) $ and iso$ for the calorimetric isolation option (isolation opt) $.

	data: bhmu0h		MC: ztopei	
	N_{event}	$\epsilon_{\text{ID}}\pm$ error (%)	N_{event}	$\epsilon_{\text{ID}}\pm$ error (%)
$N_{\text{stub hits}} > 2$		92.33 ± 0.48		95.82 ± 0.09
	2815		45023	
Δx_{BMU}	2790	99.11 ± 0.18	44965	99.87 ± 0.02
d_0	2763	98.15 ± 0.25	44820	99.55 ± 0.03
track qual opt 1	2804	99.61 ± 0.12	44992	99.93 ± 0.01
track qual opt 2	2785	98.93 ± 0.19	44877	99.68 ± 0.03
E_{em}	2740	97.34 ± 0.30	43416	96.43 ± 0.09
E_{had}	2739	97.30 ± 0.31	43762	97.20 ± 0.08
isolation opt 1	2815	100.00 ± 0.000	45023	100.00 ± 0.000
isolation opt 2	2753	97.80 ± 0.28	44409	98.64 ± 0.05
isolation opt 3	2750	97.69 ± 0.28	44223	98.22 ± 0.06
isolation opt 4	2732	97.05 ± 0.32	44223	98.22 ± 0.06
total (trq1×iso1)	2599	92.33 ± 0.50	41947	93.17 ± 0.12
total (trq1×iso2)	2547	90.48 ± 0.55	41431	92.02 ± 0.13
total (trq1×iso3)	2543	90.34 ± 0.56	41267	91.66 ± 0.13
total (trq1×iso4)	2527	89.77 ± 0.57	41267	91.66 ± 0.13
total (trq2×iso1)	2584	91.79 ± 0.52	41844	92.94 ± 0.12
total (trq2×iso2)	2535	90.05 ± 0.56	41331	91.80 ± 0.13
total (trq2×iso3)	2530	89.88 ± 0.57	41167	91.44 ± 0.13
total (trq2×iso4)	2514	89.31 ± 0.58	41167	91.44 ± 0.13

Table 3: BMU identification cut efficiencies for Gen 6 data *vs* 5.3.3 MC, where trq$ stands for the COT track quality option (track quality opt) $ and iso$ for the calorimetric isolation option (isolation opt) $.

	data: bhmu0i		MC: zewk6m	
	N_{event}	$\epsilon_{\text{ID}}\pm$ error (%)	N_{event}	$\epsilon_{\text{ID}}\pm$ error (%)
$N_{\text{stub hits}} > 2$		92.39 ± 0.66		97.90 ± 0.06
	1494		65001	
Δx_{BMU}	1485	99.40 ± 0.20	64895	99.84 ± 0.02
d_0	1475	98.73 ± 0.29	64270	98.88 ± 0.04
track qual opt 1	1488	99.60 ± 0.16	64928	99.89 ± 0.01
track qual opt 2	1479	99.00 ± 0.26	64694	99.53 ± 0.03
E_{em}	1444	96.65 ± 0.47	62626	96.35 ± 0.07
E_{had}	1458	97.59 ± 0.40	63178	97.20 ± 0.06
isolation opt 1	1494	100.00 ± 0.000	65001	100.00 ± 0.000
isolation opt 2	1454	97.32 ± 0.42	63897	98.30 ± 0.05
isolation opt 3	1458	97.59 ± 0.40	63749	98.07 ± 0.05
isolation opt 4	1439	96.32 ± 0.49	63565	97.79 ± 0.06
total (trq1×iso1)	1386	92.77 ± 0.67	60027	92.35 ± 0.10
total (trq1×iso2)	1352	90.48 ± 0.55	59088	90.90 ± 0.11
total (trq1×iso3)	1356	90.76 ± 0.75	58963	90.71 ± 0.11
total (trq1×iso4)	1340	89.69 ± 0.79	58809	90.47 ± 0.12
total (trq2×iso1)	1379	92.30 ± 0.69	59837	92.06 ± 0.11
total (trq2×iso2)	1346	90.09 ± 0.77	58908	90.63 ± 0.11
total (trq2×iso3)	1349	90.29 ± 0.77	58781	90.43 ± 0.12
total (trq2×iso4)	1334	89.29 ± 0.80	58630	90.20 ± 0.12

Table 4: BMU identification cut efficiencies for Gen 6 data *vs* 6.1.3 MC, where trq\$ stands for the COT track quality option (track quality opt) \$ and iso\$ for the calorimetric isolation option (isolation opt) \$.

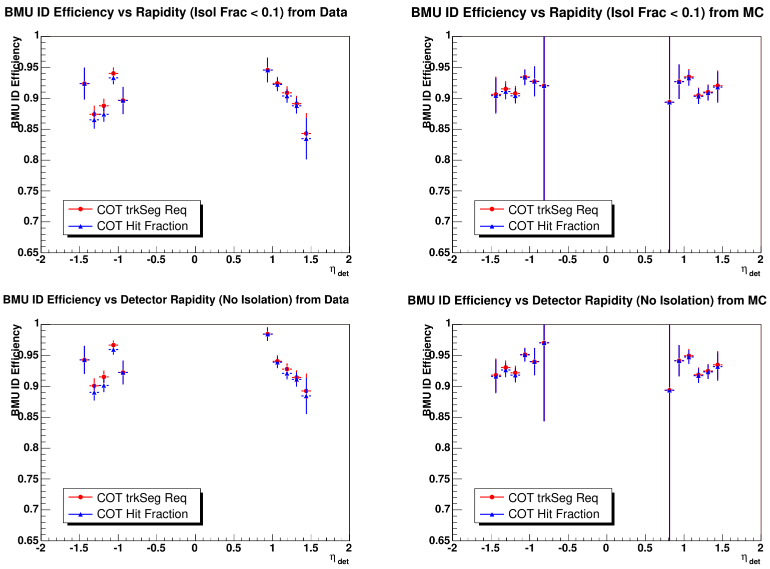

Figure 35: BMU ID efficiency *vs* detector rapidity from data (left) or MC (right), comparing the COT track quality cut options and the least/most luminosity-dependent calorimetric isolation cut options.

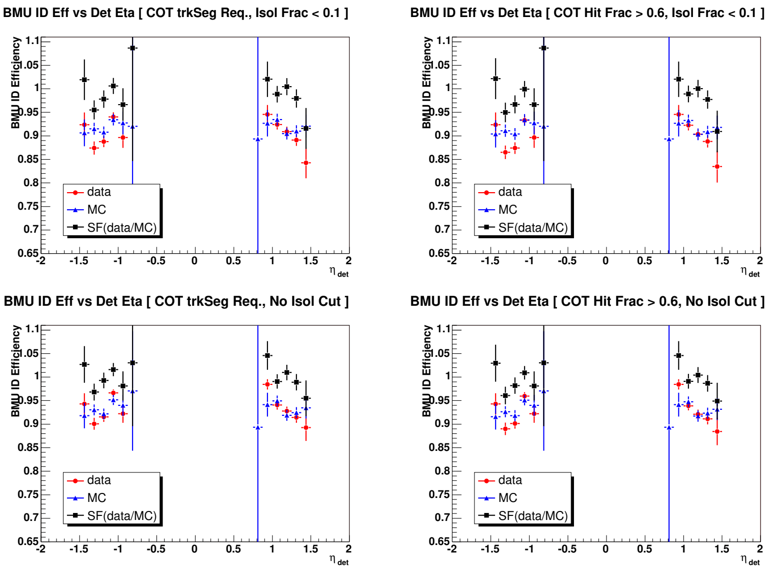

Figure 36: BMU ID efficiency and scale factor *vs* detector rapidity for COT track quality cut options and the least/most luminosity-dependent calorimetric isolation cut options.

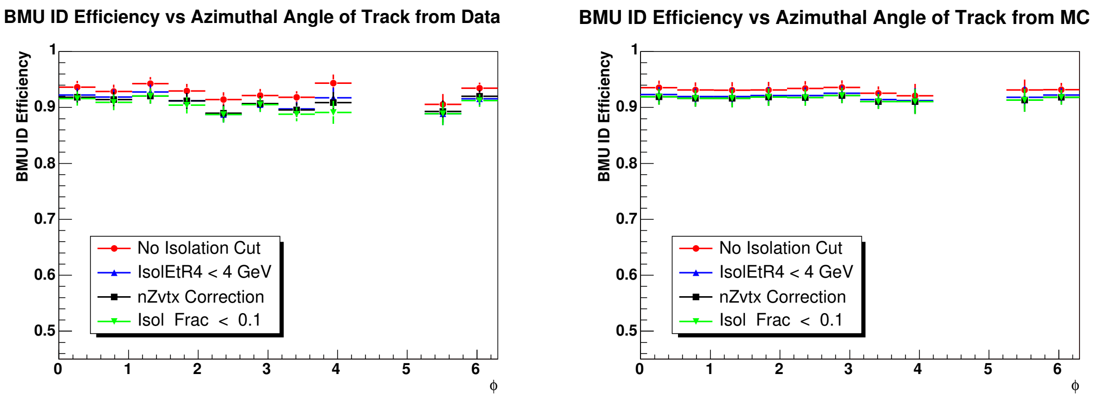

Figure 37: BMU total (trq1) ID efficiency *vs* ϕ from data (left) or MC (right), comparing all the calorimetric isolation cut options.

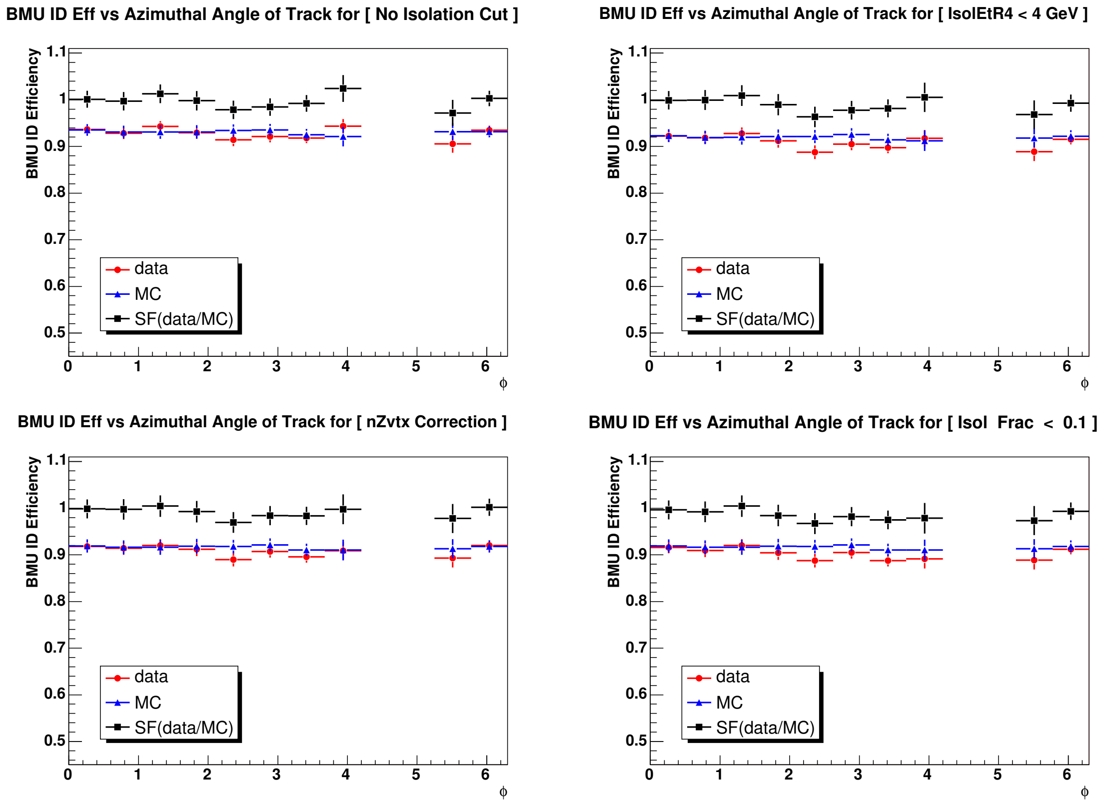

Figure 38: BMU total (trq1) ID efficiency and scale factor *vs* ϕ for each calorimetric isolation cut options.

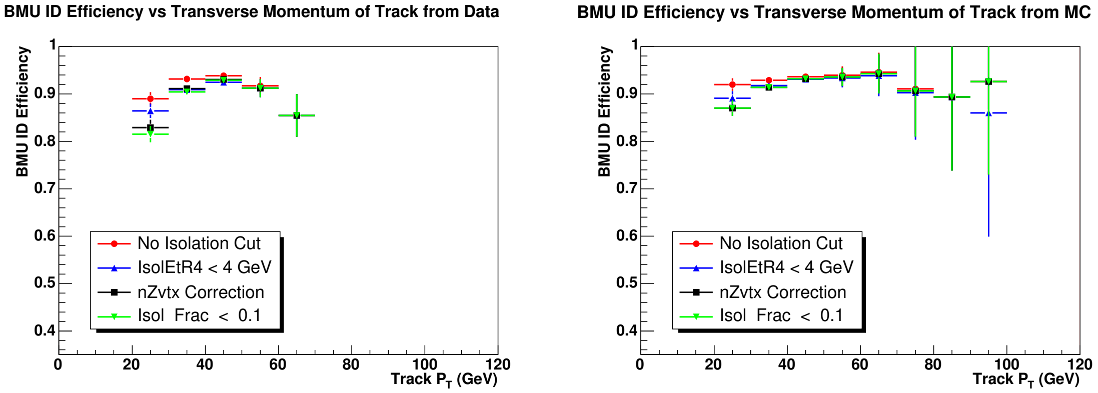

Figure 39: BMU total (trq1) ID efficiency *vs* track p_t from data (left) or MC (right), comparing all the calorimetric isolation cut options.

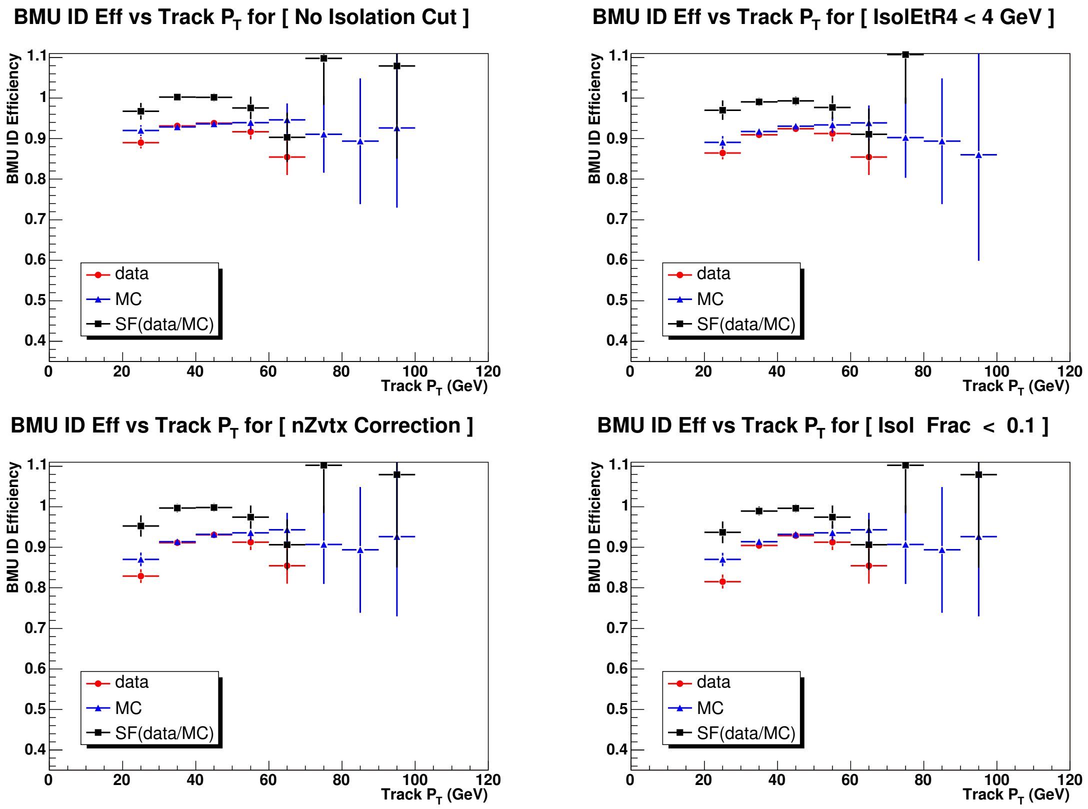

Figure 40: BMU total (trq1) ID efficiency and scale factor *vs* track p_t for each calorimetric isolation cut options.

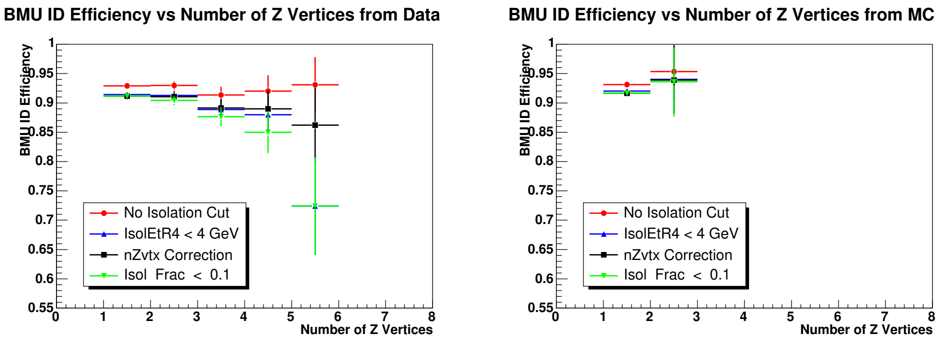

Figure 41: BMU total (trq1) ID efficiency *vs* number of Z vertices from data (left) or MC (right), comparing all the calorimetric isolation cut options.

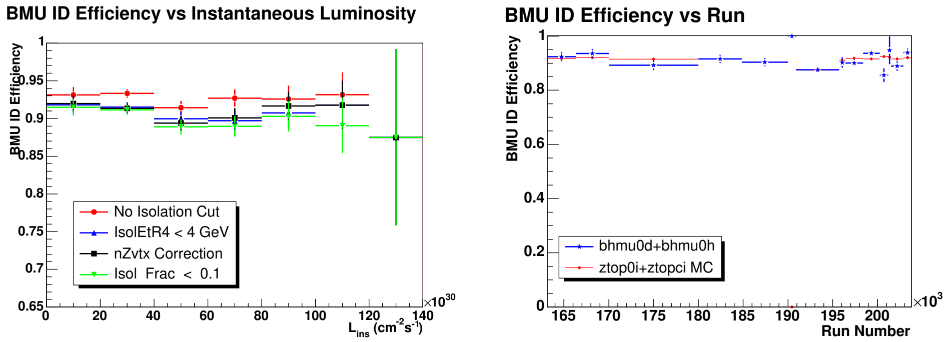

Figure 42: BMU total (trq1) ID efficiency *vs* instantaneous luminosity, comparing all the calorimetric isolation cut options (left); BMU total (trq1) ID efficiency *vs* run range (right).

	bhmu0d / ztop0i	bhmu0h / ztopei
$N_{\text{stub hits}} > 2$	0.9170 ± 0.0082	0.9636 ± 0.0051
trq1 $\times$ iso1	1.0041 ± 0.0069	0.9910 ± 0.0055
trq1 $\times$ iso2	0.9970 ± 0.0077	0.9832 ± 0.0062
trq1 $\times$ iso3	1.0007 ± 0.0078	0.9856 ± 0.0062
trq1 $\times$ iso4	0.9959 ± 0.0080	0.9794 ± 0.0064
trq2 $\times$ iso1	0.9968 ± 0.0073	0.9877 ± 0.0057
trq2 $\times$ iso2	0.9895 ± 0.0081	0.9810 ± 0.0063
trq2 $\times$ iso3	0.9933 ± 0.0082	0.9829 ± 0.0064
trq2 $\times$ iso4	0.9884 ± 0.0083	0.9767 ± 0.0065

Table 5: BMU identification scale factors for Gen 5 or Gen 6 data *vs* 5.3.3 MC.

	bhmu0h / zewk6m	bhmu0i / zewk6m
$N_{\text{stub hits}} > 2$	0.9431 ± 0.0050	0.9438 ± 0.0068
trq1 $\times$ iso1	0.9998 ± 0.0055	1.0046 ± 0.0073
trq1 $\times$ iso2	0.9953 ± 0.0062	0.9955 ± 0.0084
trq1 $\times$ iso3	0.9959 ± 0.0063	1.0006 ± 0.0084
trq1 $\times$ iso4	0.9922 ± 0.0064	0.9914 ± 0.0088
trq2 $\times$ iso1	0.9972 ± 0.0057	1.0027 ± 0.0076
trq2 $\times$ iso2	0.9937 ± 0.0063	0.9941 ± 0.0086
trq2 $\times$ iso3	0.9939 ± 0.0064	0.9985 ± 0.0086
trq2 $\times$ iso4	0.9901 ± 0.0066	0.9899 ± 0.0090

Table 6: BMU identification scale factors for Gen 6 data *vs* 6.1.3 MC.

5.3 Identification Scale Factor

BMU identification data/MC scale factors are listed in Table 5 for the Gen 5 or Gen 6 run range and in Table 6 for the Gen 6 run range.

6 Overall Scale Factor

The overall (reconstruction $\times$ identification) scale factors for all BMU are listed in Table 7 for the Gen 5 or Gen 6 run range and in Table 8 for the Gen 6 run range. The overall (reconstruction $\times$ [$N_{\text{stub hits}} > 2$] $\times$ identification) scale factors for BMU with $N_{\text{stub hits}} > 2$ are listed in Table 9 for the Gen 5 or Gen 6 run range and in Table 10 for the Gen 6 run range.

	bhmu0d / ztop0i	bhmu0h / ztopei
trq1 $\times$ iso1	1.1106 ± 0.0096	1.0993 ± 0.0077
trq1 $\times$ iso2	1.1028 ± 0.0103	1.0907 ± 0.0082
trq1 $\times$ iso3	1.1069 ± 0.0104	1.0933 ± 0.0083
trq1 $\times$ iso4	1.1015 ± 0.0105	1.0865 ± 0.0084
trq2 $\times$ iso1	1.1071 ± 0.0100	1.1020 ± 0.0076
trq2 $\times$ iso2	1.0991 ± 0.0107	1.0945 ± 0.0082
trq2 $\times$ iso3	1.1032 ± 0.0107	1.0967 ± 0.0082
trq2 $\times$ iso4	1.0978 ± 0.0109	1.0898 ± 0.0084

Table 7: BMU overall (reconstruction $\times$ identification) scale factors for Gen 5 or Gen 6 data *vs* 5.3.3 MC.

	bhmu0h / zewk6m	bhmu0i / zewk6m
trq1 × iso1	1.1235 ± 0.0082	1.1204 ± 0.0109
trq1 × iso2	1.1186 ± 0.0087	1.1103 ± 0.0118
trq1 × iso3	1.1192 ± 0.0088	1.1159 ± 0.0118
trq1 × iso4	1.1150 ± 0.0089	1.1057 ± 0.0121
trq2 × iso1	1.1276 ± 0.0078	1.1394 ± 0.0102
trq2 × iso2	1.1237 ± 0.0084	1.1297 ± 0.0112
trq2 × iso3	1.1239 ± 0.0084	1.1346 ± 0.0112
trq2 × iso4	1.1196 ± 0.0086	1.1249 ± 0.0115

Table 8: BMU overall (reconstruction × identification) scale factors for Gen 6 data *vs* 6.1.3 MC.

	bhmu0d / ztop0i	bhmu0h / ztopei
trq1 × iso1	1.0184 ± 0.0127	1.0593 ± 0.0093
trq1 × iso2	1.0112 ± 0.0131	1.0510 ± 0.0097
trq1 × iso3	1.0150 ± 0.0132	1.0535 ± 0.0097
trq1 × iso4	1.0101 ± 0.0132	1.0469 ± 0.0098
trq2 × iso1	1.0152 ± 0.0129	1.0618 ± 0.0093
trq2 × iso2	1.0078 ± 0.0133	1.0546 ± 0.0097
trq2 × iso3	1.0116 ± 0.0134	1.0567 ± 0.0097
trq2 × iso4	1.0067 ± 0.0134	1.0501 ± 0.0098

Table 9: BMU overall (reconstruction × $[\ N_{\text{stub hits}} > 2\ ]$ × identification) scale factors for Gen 5 or Gen 6 data *vs* 5.3.3 MC.

	bhmu0h / zewk6m	bhmu0i / zewk6m
trq1 × iso1	1.0596 ± 0.0095	1.0574 ± 0.0128
trq1 × iso2	1.0549 ± 0.0099	1.0479 ± 0.0134
trq1 × iso3	1.0555 ± 0.0100	1.0532 ± 0.0134
trq1 × iso4	1.0516 ± 0.0101	1.0435 ± 0.0136
trq2 × iso1	1.0634 ± 0.0092	1.0753 ± 0.0123
trq2 × iso2	1.0597 ± 0.0096	1.0661 ± 0.0130
trq2 × iso3	1.0599 ± 0.0097	1.0708 ± 0.0130
trq2 × iso4	1.0559 ± 0.0098	1.0616 ± 0.0133

Table 10: BMU overall (reconstruction × $[\ N_{\text{stub hits}} > 2\ ]$ × identification) scale factors for Gen 6 data *vs* 6.1.3 MC.

7 Z Cross-Section Measurement

To verify BMU we measure the production cross-section of $Z^0 \to \mu^+\mu^-$ in $p\bar{p}$ collisions at $\sqrt{s} = 1.96$ TeV with CMUP+BMU and CMX+BMU with Gen 5 and Gen 6 separated, using the formula

$$N_{obs} = \sigma \cdot \mathcal{L}_{int} \cdot \frac{N_o}{N_i}_{\text{MC}} \cdot \epsilon_{trg} \cdot \epsilon_{vtx} \cdot f_{\text{CMUP/CMX}} \cdot f_{\text{BMU}} + N_b$$

where

N_{obs} stands for the number of observed data events;

$\sigma \equiv \sigma(p\bar{p} \to Z^0 \to \mu^+\mu^-)$;

$\mathcal{L}_{int}$ is as described in Section 3;

$\epsilon_{raw} \equiv \frac{N_o}{N_i}_{\text{MC}}$ is the raw acceptance of signal as estimated with the MC samples described in Section 3;

ϵ_{trg} is as described in Section 3;

$\epsilon_{vtx} = 0.9555 \pm 0.0004$ (stat) ± 0.0031 (syst) is taken from [9];

$f_{\text{CMUP/CMX}}$ is as described in Section 3;

f_{BMU} is as described in Section 6;

N_b stands for the number of background events, assumed negligible¶ for now.

Results are summarized below, where the corrected signal acceptance $\epsilon_{corr} \equiv \epsilon_{raw} \cdot \epsilon_{trg} \cdot \epsilon_{vtx} \cdot f_{\text{CMUP/CMX}} \cdot f_{\text{BMU}}$:

For Gen 5 CMUP+BMU:

$\epsilon_{raw} = 0.0200 \pm 0.0001$;
$\epsilon_{corr} = 0.0153 \pm 0.0006$;
$N_{obs} = 980$;
$\sigma(p\bar{p} \to Z^0 \to \mu^+\mu^-) = 260.50 \pm 8.32$ (stat) ± 9.54 (syst) ± 15.37 (lumi) pb.

For Gen 6 CMUP+BMU:

$\epsilon_{raw} = 0.0193 \pm 0.0001$;
$\epsilon_{corr} = 0.0151 \pm 0.0004$;
$N_{obs} = 1736$;
$\sigma(p\bar{p} \to Z^0 \to \mu^+\mu^-) = 260.92 \pm 6.26$ (stat) ± 7.66 (syst) ± 15.39 (lumi) pb.

For Gen 5 CMX+BMU:

$\epsilon_{raw} = 0.0087 \pm 0.0001$;
$\epsilon_{corr} = 0.0079 \pm 0.0003$;
$N_{obs} = 448$;
$\sigma(p\bar{p} \to Z^0 \to \mu^+\mu^-) = 247.29 \pm 11.68$ (stat) ± 9.54 (syst) ± 14.59 (lumi) pb.

¶We observe zero same-sign CMUP/CMX+BMU events; since QCD fake background is insensitive to charge sign, such an observation indicates negligible QCD fake background in the opposite-sign signal region. SM opposite-sign dimuon background processes have negligbly small cross-sections in $81 < M_{\mu\mu} < 101$ GeV.

For Gen 6 CMX+BMU:

$$\epsilon_{raw} = 0.0085 \pm 0.0001;$$
$$\epsilon_{corr} = 0.0077 \pm 0.0002;$$
$$N_{obs} = 791;$$
$$\sigma(p\bar{p} \to Z^0 \to \mu^+\mu^-) = 251.04 \pm 8.93 \text{ (stat) } \pm 7.86 \text{ (syst) } \pm 14.81 \text{ (lumi) pb.}$$

Good agreement with the SM prediction of $\sigma(p\bar{p} \to Z^0 \to \ell^+\ell^-) = 251.3 \pm 5.0$ pb [11] is observed.

8 Conclusion

We have made the *first* investigation of CDF II intermediate muon, *a.k.a.* BMU, reconstruction and identification using Gen 5 and Gen 6 high p_t muon data and $Z \to \mu\mu$ MC samples and worked out good BMU selection criteria and the associated data/MC scale factors that analyses, especially those in need of muon acceptance, should consider to use.

A Reconstruction Efficiencies for Reference

The reconstruction efficiencies for forced BMU fiducial distance requirement of

x-fid$_{\text{BMU}} < 0$ cm;

z-fid$_{\text{BMU}} < 0$ cm;

in both data and MC are provided below.

with the 1st COT cut option:
(axial and stereo segments)

$\epsilon_{\text{REC}} \pm$ error (%)	muons	tracks	sample
93.8 ± 0.7	1079	1150	data:bhmu0d
92.5 ± 0.6	1899	2052	data:bhmu0h
93.0 ± 0.5	2978	3202	data:bhmu0(d+h)
86.9 ± 0.1	47566	54724	MC:ztop8i
87.3 ± 0.2	25250	28927	MC:ztop0i
87.0 ± 0.2	38891	44691	MC:ztopci
87.0 ± 0.2	38743	44537	MC:ztopei
87.0 ± 0.1	150450	172879	MC:Gen 5
85.8 ± 0.2	32616	38000	MC:zewk6m
85.8 ± 0.2	32616	38000	MC:Gen 6

with the 2nd COT cut option:
(hit fraction)

$\epsilon_{\text{REC}} \pm$ error (%)	muons	tracks	sample
94.1 ± 0.7	1077	1144	data:bhmu0d
93.0 ± 0.6	1896	2038	data:bhmu0h
93.4 ± 0.4	2973	3182	data:bhmu0(d+h)
86.9 ± 0.1	47602	54776	MC:ztop8i
87.3 ± 0.2	25270	28957	MC:ztop0i
87.0 ± 0.2	38944	44756	MC:ztopci
87.0 ± 0.2	38778	44575	MC:ztopei
87.0 ± 0.1	150594	173064	MC:Gen 5
85.8 ± 0.2	32600	37986	MC:zewk6m
85.8 ± 0.2	32600	37986	MC:Gen 6

B BMU-Fiducial CMIO

We select BMU-fiducial CMIO with the following cuts:

1. track $p_t > 20$ GeV/c;
2. track fiducial to the BMU chamber;
3. track $|z_0| < 60$ cm;
4. track $|d_0| < 0.(0)2$ cm if with (silicon +) COT hits attached;
5. on COT track quality:

   opt 1: COT axial/stereo track segments with at least 5 hits:
   $N_{\text{Ax trkSegs}} \geq 1$ and $N_{\text{St trkSegs}} \geq 2$ for $|\eta_{\text{det}}| < 1.25$;
   $N_{\text{Ax trkSegs}} \geq 1$ and $N_{\text{St trkSegs}} \geq 1$ for $|\eta_{\text{det}}| \geq 1.25$;
   opt 2: COT hit fraction > 0.6;
6. $E_{em} < 2 + \max(0, 0.0115 \times (p - 100))$ GeV;
7. $E_{had} < 6 + \max(0, 0.028 \times (p - 100))$ GeV;
8. $E_{em} + E_{had} > 0.1$ GeV;
9. on calorimetric isolation:

   opt 1: no requirement;
   opt 2: $E_t^{\text{iso4}} < 4$ GeV;
   opt 3: $(E_t^{\text{iso4}} - 0.35 \times (N_{\text{vtx}} - 1))/p_t < 0.1$;
   opt 4: $E_t^{\text{iso4}}/p_t < 0.1$.

	data: bhmu0d		MC: ztop0i	
	N_{event}	$\epsilon_{\text{ID}}\pm$ error (%)	N_{event}	$\epsilon_{\text{ID}}\pm$ error (%)
	1911		35804	
d_0	1844	96.49 ± 0.42	35568	99.34 ± 0.04
track quality opt 1	1871	97.91 ± 0.33	35746	99.84 ± 0.02
E_{em}	1832	95.87 ± 0.46	34485	96.32 ± 0.10
E_{had}	1860	97.33 ± 0.37	34840	97.31 ± 0.09
$E_{em} + E_{had}$	1840	96.28 ± 0.43	35354	98.74 ± 0.06
isolation opt 1	1911	100.00 ± 0.000	35804	100.00 ± 0.000
isolation opt 4	1830	95.76 ± 0.46	35142	98.15 ± 0.07
total (trq1×iso1)	1694	88.64 ± 0.73	32878	91.83 ± 0.14
total (trq1×iso4)	1650	86.34 ± 0.79	32348	90.35 ± 0.16

Table 11: BMU-fiducial CMIO cut efficiencies for 5.3.3 data *vs* 5.3.3 MC, where trq$ stands for the COT track quality option (track quality opt) $ and iso$ for the calorimetric isolation option (isolation opt) $.

	data: bhmu0h		MC: ztopei		MC: zewk6m	
	N_{event}	$\epsilon_{\text{ID}}\pm$ error (%)	N_{event}	$\epsilon_{\text{ID}}\pm$ error (%)	N_{event}	$\epsilon_{\text{ID}}\pm$ error (%)
	3286		53845		77250	
d_0	3131	95.28 ± 0.37	53575	99.50 ± 0.03	76326	98.80 ± 0.04
track qual opt 1	3198	97.32 ± 0.28	53775	99.87 ± 0.02	77084	99.79 ± 0.02
E_{em}	3173	96.56 ± 0.32	51868	96.33 ± 0.08	74335	96.23 ± 0.07
E_{had}	3180	96.77 ± 0.31	52291	97.11 ± 0.07	75036	97.13 ± 0.06
$E_{em} + E_{had}$	3146	95.74 ± 0.35	53175	98.76 ± 0.05	76262	98.72 ± 0.04
isolation opt 1	3286	100.00 ± 0.000	53845	100.00 ± 0.000	77250	100.00 ± 0.000
isolation opt 4	3150	95.86 ± 0.35	52809	98.08 ± 0.06	75396	97.60 ± 0.06
total (trq1×iso1)	2866	87.22 ± 0.58	49493	91.92 ± 0.12	70367	91.09 ± 0.10
total (trq1×iso4)	2783	84.69 ± 0.63	48677	90.40 ± 0.13	68894	89.18 ± 0.11

Table 12: BMU identification cut efficiencies for 6.1.2 data *vs* 5.3.3/6.1.3 MC, where trq$ stands for the COT track quality option (track quality opt) $ and iso$ for the calorimetric isolation option (isolation opt) $.

BMU-fiducial CMIO identification cut efficiencies are listed in Table 11 for the Gen 5 run range and Table 12 for the Gen 6 run range.

There is apparently a 11-15% muon acceptance gain in data and 18% in MC due to the withdrawal of stub requirements. Identification cut efficiencies are generally worse than with the BMU stub requirements, however, indicating that stubless BMU-fiducial CMIO tend to have bad COT track quality and bad isolation.

C Crosscheck ID Cuts and Efficiencies for 5.3.3

For 5.3.3 generation we use the high-P_T muon data sample **bhmu0d**, corresponding to an integrated luminosity of 346.9 pb^{-1} for CMUP muons and of 326.8 pb^{-1} for CMX muons, and the PYTHIA generated Monte Carlo sample **ztop8i**. We apply the following two "standard" cuts for all muons:

- $P_T > 20$ GeV/c
- $|Z_0| < 60$ cm

P_T is the transverse momentum of the muons and Z_0 is the vertex position. We select muon pairs where one leg, CMUP or CMX, is always a tight central muon, as defined in CDF note 7956, and the other leg is a track fiducial to the BMU chambers and having a BMU stub. In addition, we apply the following three "standard" cuts for all muon pairs, trying to isolate the process $Z \to \mu\mu$ as much as possible:

- 81 GeV/c^2 $< M_{\mu\mu} <$ 101 GeV/c^2
- $|Z_0^{(1)} - Z_0^{(2)}| < 4$ cm
- $Q_1 Q_2 = -1$, where Q is the charge of the muon.

The reason for this is that, when the above cuts are applied to the data, the Z peak in the ivariant mass $M_{\mu\mu}$ spectrum, expected at 91.2 GeV/c^2, offers a reliable signal for the quality of identification and tracking of BMU muons. In particular, by removing the last three cuts and applying once the inverse track pair matching cut ($|Z_0^{(1)} - Z_0^{(2)}| > 4$ cm) and once the same sign cut ($Q_1 Q_2 = +1$) without any other requirement on the

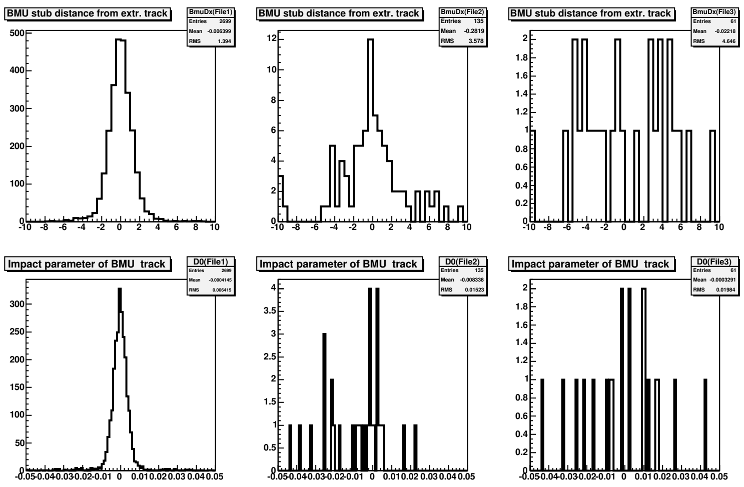

Figure 43: Comparison of the Δx of muon tracks in the BMU chambers (top) and of the impact parameter of the BMU tracks (bottom) for the signal (left), for the unmatched-track background (middle) and for the same-sign background (right).

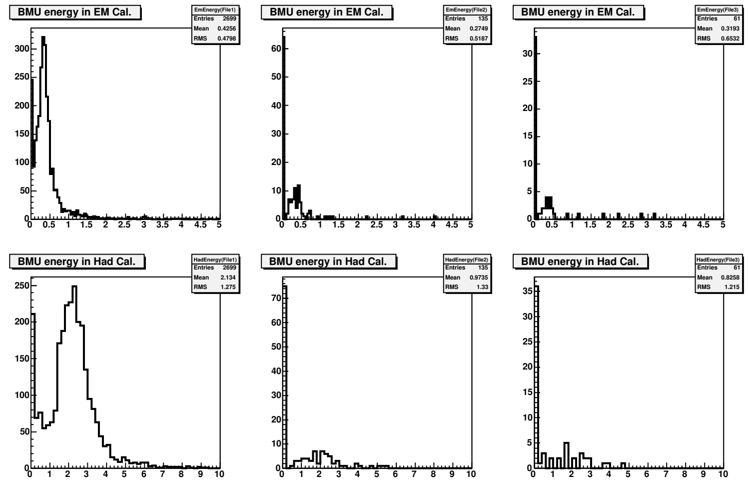

Figure 44: Comparison of the energy deposits in the EM calorimeter (top) and in the hadronic calorimeter (bottom) for the signal (left), for the unmatched-track background (middle) and for the same-sign background (right).

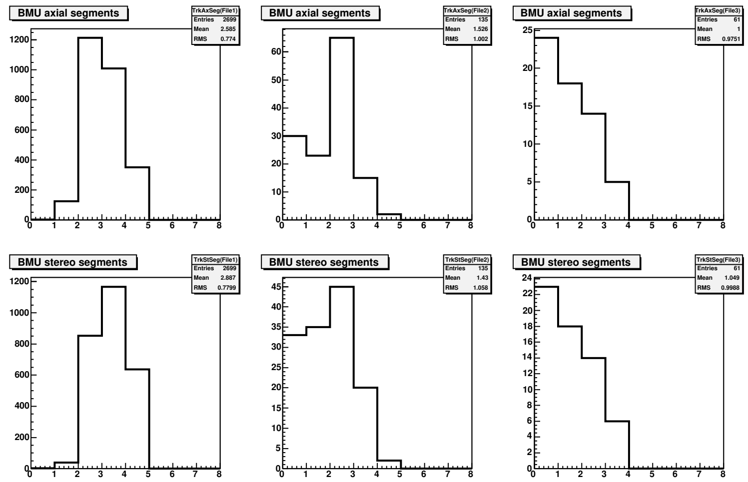

Figure 45: Comparison of the number of COT axial segments (top) and of the COT stereo segments (bottom) for the signal (left), for the unmatched-track background (middle) and for the same-sign background (right).

BMU leg, but always selecting a tight muon for the central leg, we define two sets of "background" to the $Z \to \mu\mu$ process which are likely to contain "bad" BMU muons. The comparisons between these backgrounds and the $Z \to \mu\mu$ signal help us define ranges of reliability of variables associated with BMU muons, where cuts should be applied.

Figures 43 - 45 show the comparison between the signal (left windows), the unmatched track pair background passing the cut $|\mathrm{Z}_0^{(1)} - \mathrm{Z}_0^{(2)}| > 4$ cm (middle windows) and the same sign background (right windows) for six BMU-associated variables that we found most important in reducing the width of the Z peak, i.e. selecting higher quality BMU tracks. Figure 43 shows the transverse distance $\Delta \mathrm{x}_{\mathrm{BMU}}$ between the BMU stub and the extrapolated track and the impact parameter d_0 of the track. Figure 44 shows the energy deposits of the track in the EM and hadronic calorimeters. Figure 45 shows the numbers of axial and stereo segments per track in the COT. All three Figures show data from the **bhmu0d** sample.

Based on these comparisons we deduce the cuts we need to impose on the variables shown in the Figures. These cuts are listed in Table 13 with their efficiencies $\varepsilon \pm \delta\varepsilon$ for data and Monte Carlo and the corresponding scale factors SF$\pm\delta$SF. However, at present, a major concern is to increase the overall ID efficiency of CDF muons. Therefore we also give another set of looser cuts listed in Table 14 with their efficiencies for data and Monte Carlo and the corresponding scale factors. The "sliding" for energy deposition in the calorimeters is given by

$$\mathrm{E_{em}} = 2 + \max\{0, (\mathrm{p} - 100) \cdot 0.0115\} \text{ GeV} \tag{1}$$

$$\mathrm{E_{had}} = 6 + \max\{0, (\mathrm{p} - 100) \cdot 0.028\} \text{ GeV} \tag{2}$$

The cut on the number of COT stereo segments in Table 14 depends on the pseudorapidity of the BMU track: it is required to be greater than 1 for $1 < |\eta| < 1.25$ and greater than 0 for $1.25 < |\eta| < 1.5$ (see the previous discussion of gen 6 data). For analyses mostly concerned about muon quality we recommend the cuts of Table 13, whereas for analyses mostly concerned about statistics we recommend the cuts of Table 14.

Variable	Cut	$\varepsilon_{\mathrm{data}}$ (%)	$\delta\varepsilon_{\mathrm{data}}$ (%)	$\varepsilon_{\mathrm{MC}}$ (%)	$\delta\varepsilon_{\mathrm{MC}}$ (%)	SF (%)	δSF (%)
$\lvert\Delta \mathrm{x}_{\mathrm{BMU}}\rvert$	< 4 cm	97.63	2.67	95.39	0.50	102.35	2.85
$\mathrm{E_{em}}$	< 2 GeV + slide	97.15	2.66	96.58	0.62	100.59	2.83
$\mathrm{E_{had}}$	< 6 GeV + slide	97.66	2.67	97.32	0.51	100.35	2.79
Ax Seg	> 1	95.29	2.63	94.06	0.50	101.31	2.85
St Seg	> 1	98.41	2.69	99.15	0.52	99.25	2.76
$\lvert\mathrm{d}_0\rvert$	$< 0.02, 0.2$ cm	98.33	2.69	99.36	0.52	98.96	2.76
Overall		86.48	2.44	87.21	0.47	99.16	2.85

Table 13: Tight ID cuts for BMU muons with the respective efficiencies and scale factors.

Variable	Cut	$\varepsilon_{\rm data}$ (%)	$\delta\varepsilon_{\rm data}$ (%)	$\varepsilon_{\rm MC}$ (%)	$\delta\varepsilon_{\rm MC}$ (%)	SF (%)	δSF (%)
$\lvert\Delta x_{\rm BMU}\rvert$	< 9 cm	99.59	2.71	99.87	0.52	99.72	2.76
E_{em}	< 2 GeV + slide	97.15	2.66	96.58	0.62	100.59	2.83
E_{had}	< 6 GeV + slide	97.66	2.67	97.32	0.51	100.35	2.79
Ax Seg	> 0	99.93	2.72	100	0.52	99.93	2.77
St Seg	$> 1, 0$	99.33	2.70	99.75	0.52	99.58	2.76
$\lvert d_0\rvert$	$< 0.02, 0.2$ cm	98.33	2.69	99.36	0.52	98.96	2.76
Overall		92.88	2.57	93.03	0.49	99.84	2.81

Table 14: Loose ID cuts for BMU muons with the respective efficiencies and scale factors.

Figures 46 - 48 show the overall ID efficiency $\varepsilon_{\rm data}$ as a function of the BMU P_T, η and Φ for the tight cuts of Table 13. Figures 49 - 51 show the overall ID efficiency $\varepsilon_{\rm data}$ as a function of the BMU P_T, η and Φ for the loose cuts of Table 14. It is seen that in both cases the efficiency is flat within errors over the statistically significant bins.

In Figures 52 - 61 data histograms (in red) and Monte Carlo histograms(in blue) normalized to the data are overlaid for some important BMU-associated variables. The loose ID cuts of Table 14 are applied to both the data and the Monte Carlo, together with the standard cuts which are always assumed in effect. The comparison shows that the Monte Carlo is in good qualitative agreement with the data. One exception is the $\Delta x_{\rm BMU}$ variable shown in Figure 52. Its distribution was originally found centered at 0.2 cm, in contrast with the Monte Carlo which is centered at 0 cm. We take out this misalignment by shifting the distribution of the data by -0.2 cm.

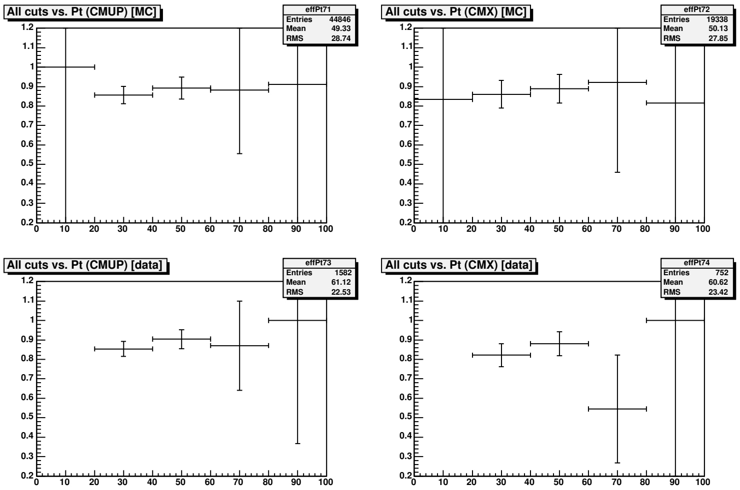

Figure 46: The overall ID efficiency of BMU muons with CMUP tight leg (left) and CMX tight leg (right) for the Monte Carlo (top) and for the data (bottom) as a function of the transverse momentum of the BMU muons. Tight ID cuts are applied on the BMU muons.

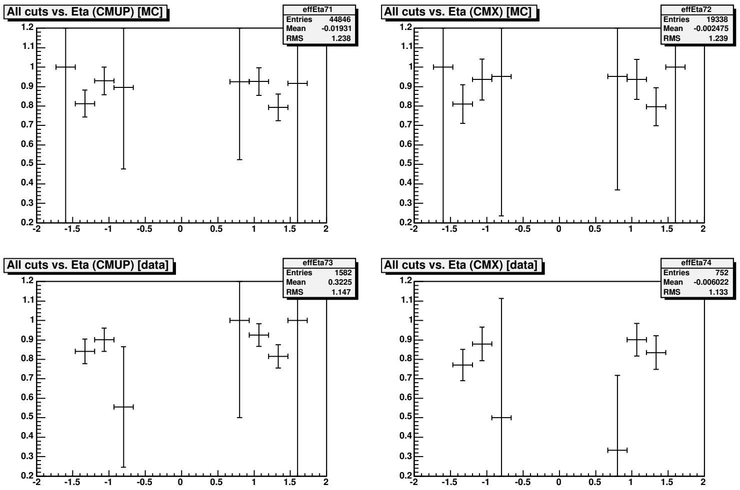

Figure 47: The overall ID efficiency of BMU muons with CMUP tight leg (left) and CMX tight leg (right) for the Monte Carlo (top) and for the data (bottom) as a function of the pseudo-rapidity of the BMU muons. Tight ID cuts are applied on the BMU muons.

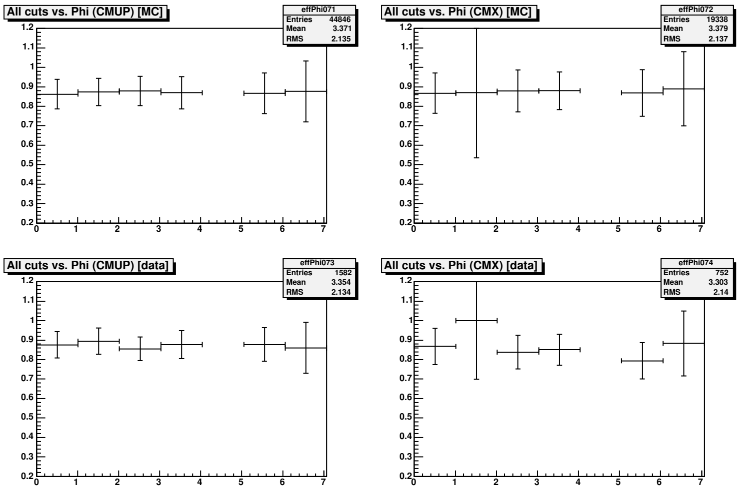

Figure 48: The overall ID efficiency of BMU muons with CMUP tight leg (left) and CMX tight leg (right) for the Monte Carlo (top) and for the data (bottom) as a function of the azimuth of the BMU muons. Tight ID cuts are applied on the BMU muons.

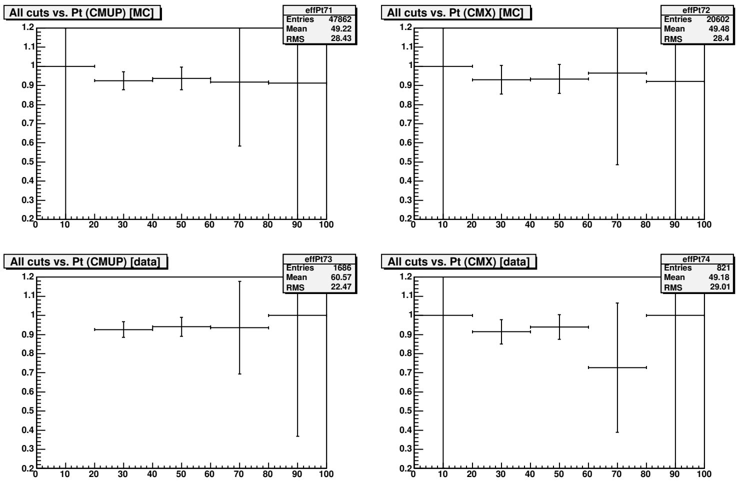

Figure 49: The overall ID efficiency of BMU muons with CMUP tight leg (left) and CMX tight leg (right) for the Monte Carlo (top) and for the data (bottom) as a function of the transverse momentum of the BMU muons. Loose ID cuts are applied on the BMU muons.

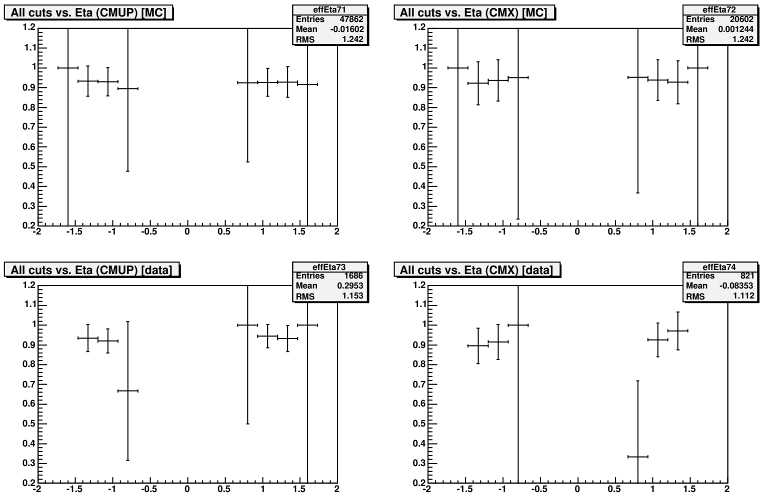

Figure 50: The overall ID efficiency of BMU muons with CMUP tight leg (left) and CMX tight leg (right) for the Monte Carlo (top) and for the data (bottom) as a function of the pseudo-rapidity of the BMU muons. Loose ID cuts are applied on the BMU muons.

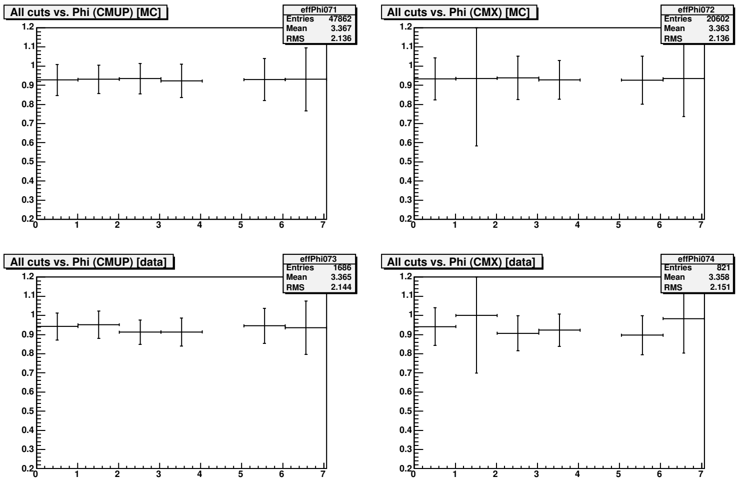

Figure 51: The overall ID efficiency of BMU muons with CMUP tight leg (left) and CMX tight leg (right) for the Monte Carlo (top) and for the data (bottom) as a function of the azimuth of the BMU muons. Loose ID cuts are applied on the BMU muons.

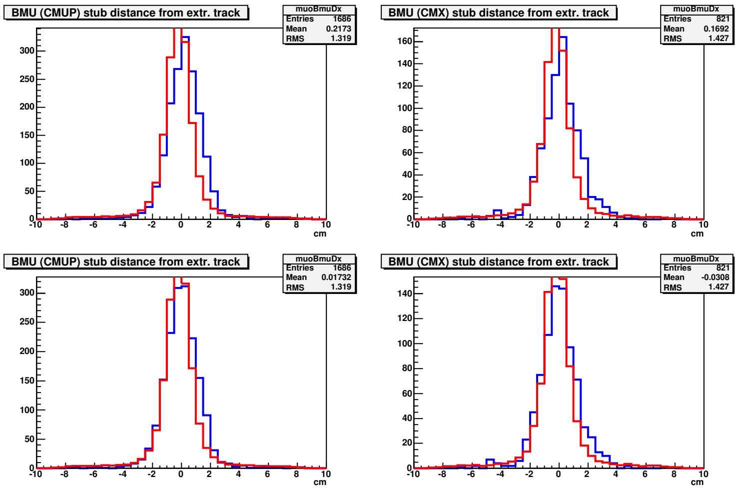

Figure 52: Comparison of data (blue) and Monte Carlo (red) scaled to the data for the Δx of muon tracks in the BMU chambers with CMUP tight leg (left) and CMX tight leg (right). The top figures show the comparison before the shift correction applied to the data. The bottom figures show the comparison after the correction.

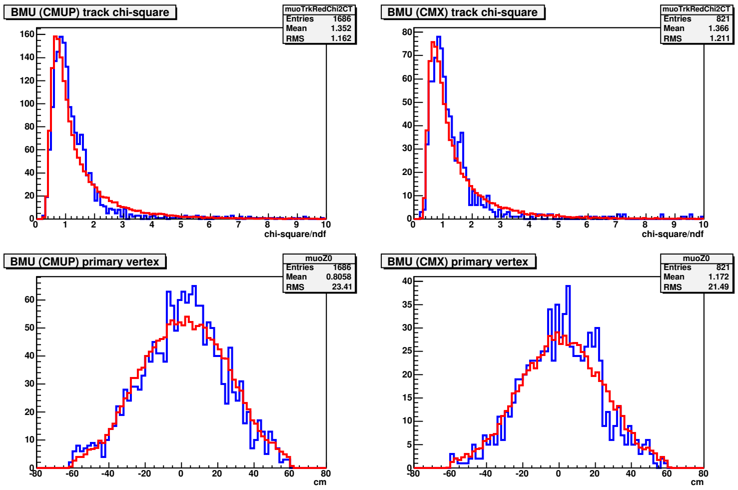

Figure 53: Comparison of data (blue) and Monte Carlo (red) scaled to the data for the BMU track χ^2 (top) and vertex Z_0 (bottom) with CMUP tight leg (left) and CMX tight leg (right).

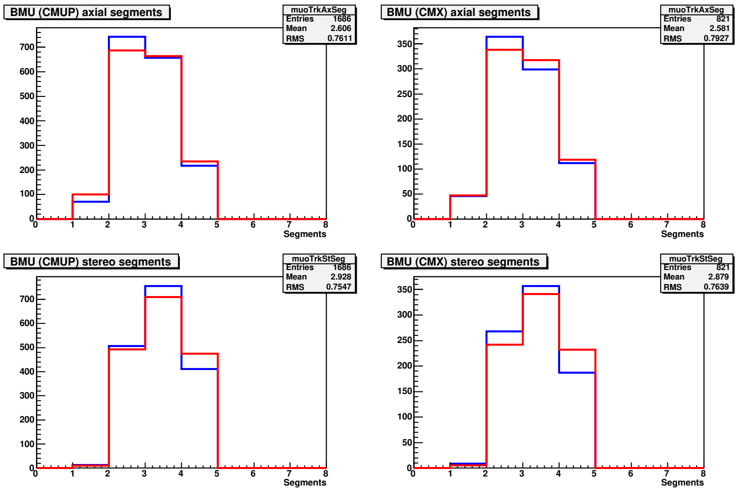

Figure 54: Comparison of data (blue) and Monte Carlo (red) scaled to the data for the COT axial (top) and stereo (bottom) segments of BMU tracks with CMUP tight leg (left) and CMX tight leg (right).

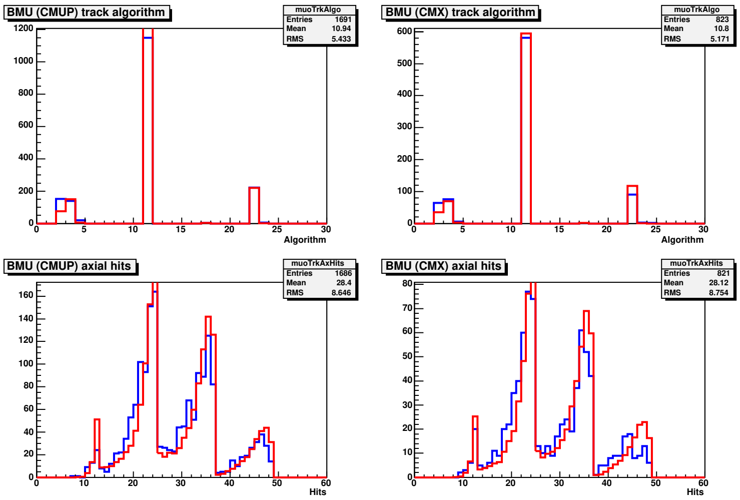

Figure 55: Comparison of data (blue) and Monte Carlo (red) scaled to the data for the algorithm (top) and the axial hits (bottom) of BMU tracks with CMUP tight leg (left) and CMX tight leg (right).

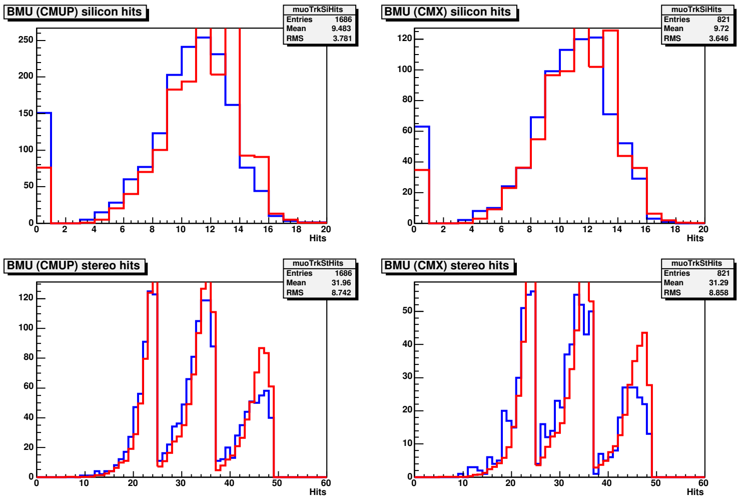

Figure 56: Comparison of data (blue) and Monte Carlo (red) scaled to the data for the silicon hits (top) and the stereo hits (bottom) of BMU tracks with CMUP tight leg (left) and CMX tight leg (right).

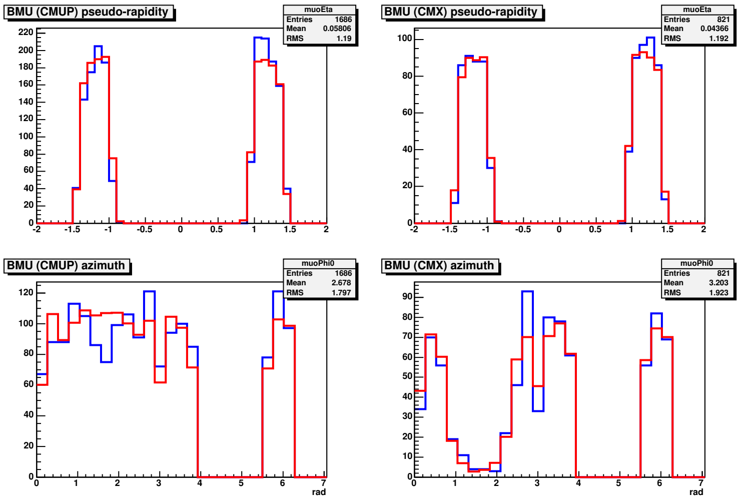

Figure 57: Comparison of data (blue) and Monte Carlo (red) scaled to the data for the pseudo-rapidity (top) and the azimuth (bottom) of BMU tracks with CMUP tight leg (left) and CMX tight leg (right).

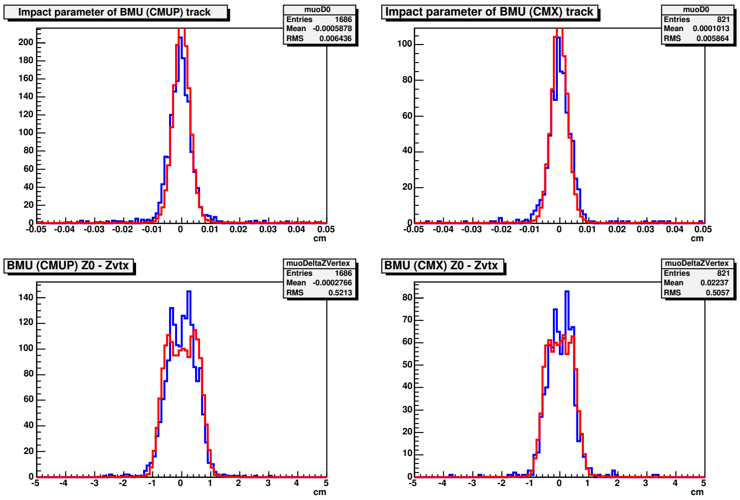

Figure 58: Comparison of data (blue) and Monte Carlo (red) scaled to the data for the impact parameter (top) and the vertex displacement (bottom) of BMU tracks with CMUP tight leg (left) and CMX tight leg (right).

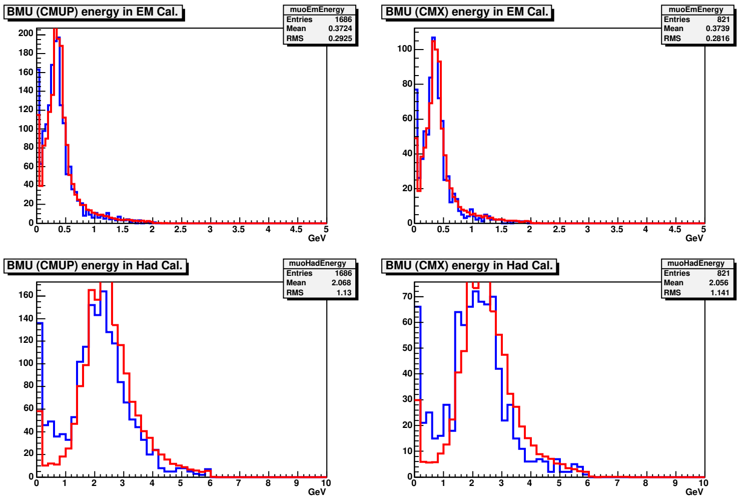

Figure 59: Comparison of data (blue) and Monte Carlo (red) scaled to the data for the energy deposits in the EM calorimeter (top) and in the hadronic calorimeter (bottom) of BMU tracks with CMUP tight leg (left) and CMX tight leg (right).

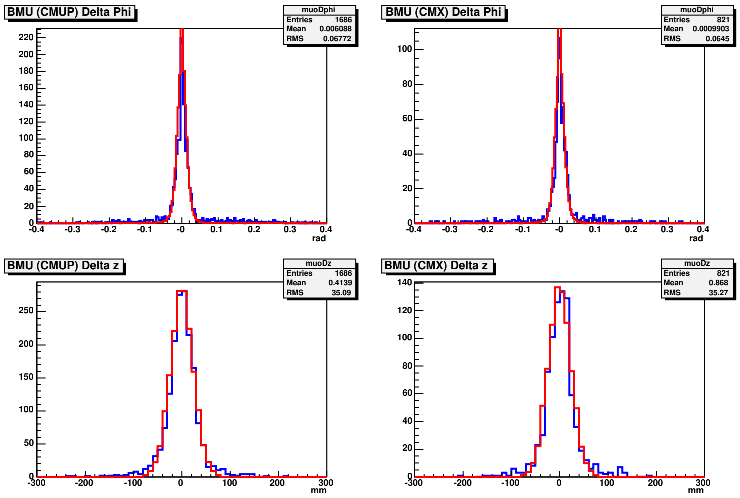

Figure 60: Comparison of data (blue) and Monte Carlo (red) scaled to the data for the Δz (top) and $\Delta\Phi$ of muon tracks in the BMU chambers with CMUP tight leg (left) and CMX tight leg (right).

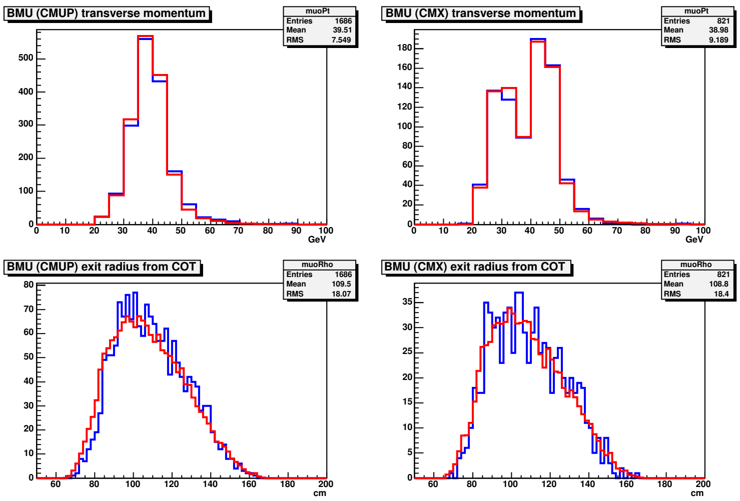

Figure 61: Comparison of data (blue) and Monte Carlo (red) scaled to the data for the transverse momentum (top) and the COT exit radius of muon tracks in the BMU chambers with CMUP tight leg (left) and CMX tight leg (right).

References

[1] The CDF II Detector Technical Design Report, the CDF II Collaboration, FERMILAB-Pub-96/390-E. Not entirely up-to-date, as usual with any detector proposal *vs* actual condition - IMU endwall scintillator counters are never built.

[2] http://www-cdf.fnal.gov/internal/dqm/goodrun/good.html

[3] http://www-cdf.fnal.gov/internal/physics/joint_physics/index.html

[4] Muon Efficiencies for Summer Analyses, Victoria Martin and David Dagenhart, CDF6610, 08/07/03.

[5] Muon Cuts and Efficiencies for 4.11 Analyses, Victoria Martin and Lucio Cerrito, CDF6825, 02/03/04.

[6] Curvature Corrections for 5.3.1, Larry Nodulman, CDF6971, 04/12/04.

[7] High P_T muons, recommended cuts and efficiencies for release 5.3.1, Victoria Martin, CDF7031, 11/02/04.

[8] High P_T Muon ID Cuts and Efficiencies for use with 5.3.1 Data and 5.3.3 MC, Victoria Martin, CDF7367, 03/06/05.

[9] Event $|Z_{vtx}| < 60$ cm Cut Acceptance for Run II (to Sep05), Willis Sakumoto, CDF7935, 11/11/05.

[10] High P_T Muon Recommended Cuts and Efficiencies for Winter 2006, Xiaojian Zhang and Ulysses Grundler, CDF7956, 11/28/05.

[11] First Measurements of Inclusive W and Z Cross Sections from Run II of the Fermilab Tevatron Collider, PRL **94** 091803 (2005).